

https://dspace.org/

Characterisation and kinetics of aptamer binding to HIV-1 subtype C gp120

Millroy, Laura

2011-03-29
http://hdl.handle.net/10539/9269

Downloaded from a DSpace repository. https://dspace.org/

Characterisation and Kinetics of Aptamer Binding to HIV-1 Subtype C gp120

Laura Millroy
0509343H

Professor R Veale
School of Molecular and Cell Biology, University of the Witwatersrand
Dr M Weinberg
School of Pathology, University of the Witwatersrand
Dr M Khati
Biosciences, CSIR and Department of Medicine, Groote Schuur Hospital and University of Cape Town

A Research Report submitted to the Faculty of Science, of the University of the Witwatersrand fulfilling the requirements of the degree Master of Science by Coursework and Research Report.

February 2010

Declaration

I declare that this thesis is my own, unaided work. It is being submitted for the degree of Masters by coursework and Research Report in the University of the Witwatersrand, Johannesburg. It has not been submitted before for any degree or examination in any other University.

Signature ----------

Date ----------

Acknowledgements

There are many people that helped me along the way to completing this research and I would like to thank each of them.

To Dr Marco Weinberg, thank you for your help and guidance along the way. Your critical review has been truly invaluable. Your wealth of knowledge and passion for science is something I will always admire.

To Dr Makobetsa Khati (Shooz), thank you for always being available to provide direction and clarity. Your passion, drive and attention to detail have pushed me to always strive for perfection.

To Professor Rob Veale, thank you for taking me on so late in this process and for providing solutions to many problems.

To the Aptamer lab, thank you for all the good times and for always being available to help or just for a good laugh. A special thanks to Grace and Thandeka for showing me the ropes and to Lia for proof reading my draft.

To Luca, thank you for helping me through the long nights and stressful moments. You are my good man in a bad storm.

To my family, thank you for being there for me when I needed help, support and a push in the right direction. A special thanks to mom for proof reading and helping me to find clarity.

Lastly I would like to thank the NRF Scarce Skills Scholarship, GDACE and the Financial Aid and Scholarships Office for funding my project.

Table of Contents

Abstract ..... **i**

List of Abbreviations ..... **ii**
List of Figures ..... **iii**
List of Tables ..... **iv**

1 Introduction **1**
1.1. Background 1
1.2. HIV Tropism and Entry 2
1.3. Entry inhibitors 4
1.4. Aptamers: A Novel Inhibitory Mechanism 7
1.4.1. Aptamers vs. Antibodies 8
1.4.2. Current and Future Prospects of Aptamer Technology 10
1.4.3. Application of Aptamer Technology: Delivery of siRNA 13
1.5. Problem Identification 13
1.6. Research Objectives 14

2 Methods **15**
2.1. Cell Maintenance 15
2.2. Selection of Aptamers 15
2.3. Oligonucleotides 15
2.4. Polymerase Chain Reaction 16
2.5. *In vitro* Transcription 17
2.6. Expression of gp120 18
2.7. Sodium Dodecyl Sulphate Polyacrylamide Gel Electrophoresis 18
2.8. Western Blot 19
2.10. BIAcore Surface Plasmon Resonance Assays 19
2.10.1. Validation of Protein Structure 20
2.10.2. Aptamer Binding to gp120 20
2.10.3. Aptamer Binding Kinetics on gp120 21
2.11. Computational Analysis of Aptamer Secondary Structure 21

3 Results **23**
3.1. PCR of Aptamer Clones 23
3.2. *In vitro* Transcription of Aptamers 24

3.3. Computational Analysis of Aptamer Secondary Structure 24
3.4. Expression and Purification of gp120 27
3.5. Validation of gp120 by Binding to IgG b12 28
3.6. Aptamers Isolated against HIV-1_{BA-L} gp120 Bound Monomeric DU151 gp120 28
3.7. Aptamers Isolated against Whole HIV-1_{CAP45} gp120 Bound to HIV-1_{CAP45} Monomeric gp120 30
3.8. Optimisation of Kinetics Using UCLA on HIV-1_{DU151} gp120 31
3.9. Further Optimisation of Kinetics on HIV-1_{DU151} gp120 35
3.10. Aptamer Binding Kinetics on HIV-1_{DU151} gp120 37
3.10.1. B84 Kinetics on HIV-1_{DU151} gp120 37
3.10.2. B65 Kinetics on HIV-1_{DU151} gp120 39
3.10.3. B11 Kinetics on HIV-1_{DU151} gp120 40
3.11. Aptamer Kinetics on HIV-1_{CAP45} gp120 41
3.11.1. P10 Kinetics on HIV-1_{CAP45} gp120 41
3.11.2. T58 Kinetics on HIV-1_{CAP45} gp120 42
3.11.3. P2 Kinetics on HIV-1_{CAP45} gp120 44

4. Discussion 45

5. Further studies 49

6. Conclusion 50

Appendix 1 51
Appendix 2 54

Reference List 58

Abstract

Aptamers are artificial nucleic acid ligands that can be engineered to bind to with high specificity to a macromolecule. Their binding specificity and small size allow for a range of therapeutic applications. One avenue of research is to develop aptamers with specific and strong affinity to the HIV-1 envelope glycoprotein gp120. Aptamers could act as novel HIV-1 entry inhibitor drugs or as targeted drug delivery systems to HIV-1 infected cells. Prior to any downstream applications, novel gp120 aptamers need to be biophysically characterised with regards to their target binding characteristics. Eight aptamers (B11, B19, B84, B65, B5, P10, P2 and T58) that have been previously isolated against gp120 and effectively block HIV-1 entry into target cells were used in this study. Secondary structures of selected anti-gp120 aptamers were computationally determined and analysed. Between one and five structures were predicted for each aptamer. The relative stability of the aptamers was analysed and B11 was shown to have the most stable structure. Using surface plasmon resonance technology aptamer binding was tested and binding kinetics was determined. Five aptamers (B11, B19, B84, B65 and B5) raised against gp120 derived from a subtype B isolate called HIV-1_{BA-L} were tested for binding to monomeric HIV-1_{DU151} gp120. Kinetic analysis of B11, B65 and B84 followed. The remaining three aptamers (P10, P2 and T58) were raised against whole HIV-1_{CAP45} pseudovirus and were tested for binding on monomeric HIV-1_{CAP45} gp120. All three were used for binding kinetic assessment on monomeric HIV-1_{CAP45} gp120. The dissociation constants were found to be similar to that of previously characterised anti-gp120 aptamers within the nanomolar range of 16.9 nM to 221 nM. Using the dissociation constant and predicted structure, P2 and B84 were identified as having the greatest potential for further characterisation.

List of Abbreviations

AIDS	acquired immune deficiency syndrome
AMD	age-related macular degeneration
AptaBiD	aptamer-facilitated biomarker discovery
ARVs	antiretrovirals
ATP	adenosine triphosphate
CD	circular dichroism
CCR5	chemokine (C-C motif) receptor 5
C-HR	C-terminal heptad repeat region of gp41
CXCR4	chemokine (C-X-C motif) receptor 4
CD4	cluster of differentiation 4
DNA	deoxyribonucleic acid
DMEM	dulbecco's modified eagle's medium
EMSA	electromobility shift assay
Env	envelope glycoprotein
gp120	120 kDa glycoprotein
gp41	41 kDa glycoprotein
HAART	highly active antiretroviral therapy
HEPES	4-(2-hydroxyethyl)-1-piperazineethanesulfonic acid
HIV	human immunodeficiency virus
HIV-1	human immunodeficiency virus type 1
kd	ligand dissociation
ka	ligand association
K_d	dissociation constant
kDa	kilodalton
mRNA	messenger RNA
NAbs	neutralising antibodies
N-HR	N-terminal heptad repeat region of gp41
PBS	phosphate buffered saline
PEG	polyethylene glycol
PCR	polymerase chain reaction
RNA	ribonucleic acid
RNAi	RNA interference
rpm	revolutions per minute
RU	response units
SDS-PAGE	sodium dodecylsulfate polyacrylamide gel electrophoresis
SELEX	systematic evolution of ligands exponential enrichment
siRNA	short interfering ribonucleic acid
SPR	surface plasmon resonance
T20	enfurvirtide, fuzeon
UV	ultra violet
ΔG	Gibbs free energy

List of Figures

Figure 1: The Progression of HIV-1 Strains and Cellular Tropism. 2
Figure 2: HIV Entry into CD4+ Cells. 3
Figure 3: Model of HIV Membrane Fusion. 4
Figure 4: *In vitro* Selection of Aptamers Using SELEX. 7
Figure 5: 2.5% Agarose Gel of Representative PCR Products Used for Transcription. 23
Figure 6: Denaturing Polyacrylamide Gel Indicating the Process of RNA Purification and Precipitation. 24
Figure 7: Predicted Secondary Structure of Aptamers by MFOLD. 26
Figure 8: 8% SDS-PAGE Indicating Purified HIV-1_{DU151} gp120 27
Figure 9: Western Blot of HIV-1_{DU151} gp120 with Positive Control 27
Figure 10: Monoclonal b12 Antibody Binding HIV-1_{DU151} gp120. 28
Figure 11: Aptamers Raised Against HIV-1_{BA-L} Binding to HIV-1_{DU151} gp120 29
Figure 12: Aptamer Binding to HIV-1_{CAP45} gp120. 31
Figure 13: UCLA Binding Kinetics on Minimum Protein Response Units. 32
Figure 14: Preparation of CM5 Chip for Kinetic Analysis of UCLA on HIV-1_{DU151} gp120. 33
Figure 15: UCLA Binding Kinetics on HIV-1_{DU151} gp120. 34
Figure 16: UCLA Binding Kinetics on 3000 RU HIV-1_{DU151} gp120 35
Figure 17: Preparation of CM5 Chip for Kinetics Experiments 36
Figure 18: B84 Binding Kinetics on HIV-1_{DU151} gp120 with Increased Concentration Limits. 38
Figure 19: B65 Binding Kinetics on HIV-1_{DU151} gp120. 39
Figure 20: B11 Binding Kinetics on HIV-1_{DU151} gp120. 40
Figure 21: P10 Binding Kinetics on HIV-1_{CAP45} gp120. 42
Figure 22: T58 Binding Kinetics on HIV-1_{CAP45} gp120. 43
Figure 23: P2 Binding Kinetics on HIV-1_{CAP45} gp120. 44

List of Tables

Table 1: Antiretroviral Drugs in Development During 2009.....6
Table 2: Nucleotide Sequences of the Common Flanking Regions (T7 and T3) and Random Internal Regions of the Selected Aptamers.....16
Table 3: Aptamer Sizes in Number of Bases.....23
Table 4: Calculated Constants and Associated Chi^2 Values for UCLA Kinetics on HIV-1_{DU151} gp120.....34
Table 5: Calculated Constants and Associated Chi^2 Values for B84 Kinetics on HIV-1_{DU151} gp120.....38
Table 6: Calculated Constants and Associated Chi^2 Values for B65 Kinetics on HIV-1_{DU151} gp120.....40
Table 7: Calculated Constants and Associated Chi^2 Values for B11 Kinetics on HIV-1_{DU151} gp120.....41
Table 8: Calculated Constants and Associated Chi^2 Values for P10 Kinetics on HIV-1_{CAP45} gp120.....42
Table 9: Calculated Constants and Associated Chi^2 Values for T58 Kinetics on HIV-1_{CAP45} gp120.....43
Table 10: Calculated Constants and Associated Chi^2 Values for P2 Kinetics on HIV-1_{CAP45} gp120.....44
Table 11: Comparison of Aptamer K_d and Most Probable Structure ΔG.....47

1 Introduction

1.1. Background

Human immunodeficiency virus (HIV) infects an estimated 33 million people worldwide (UNAIDS 2009) and is the causative agent of acquired immunodeficiency syndrome (AIDS), a global public health issue. To date numerous treatments are available that can effectively increase the life expectancy of an infected individual. Most antiretroviral treatments, both in development and on the market, are based on HIV subtype B. However, HIV subtype C is the most prevalent subtype in developing countries and is responsible for the majority of the epidemic (UNAIDS 2009). With the prevalence of non-subtype B variants and the rapid mutation rate of the virus, resistance to treatment is experienced within a couple of years causing a change in treatment plan. It has been shown that treatment naive individuals may be infected with non-subtype B strains exhibit mutations that may reduce the efficacy of current treatments (Vergne 2000). These mutations may result in individuals developing multidrug resistance faster than expected.

To combat drug resistance current treatment makes use of combinations of drugs to suppress viral replication - this is referred to as highly active retroviral therapy (HAART). The current antiretroviral drugs (ARVs) form four different classes based on their mode of action. This includes: protease inhibitors (PI), nucleoside and non-nucleoside reverse transcriptase inhibitors (NRTI and NNRTI), integrase inhibitors (II) and entry inhibitors (EI). HAART includes the use of a protease inhibitor (PI) coupled with either nucleoside reverse transcriptase inhibitors (NRTI) or non-nucleoside reverse transcriptase inhibitors (NNRTI) (Baxter 2006). Although this greatly increased the treatment success, the drugs still have to be altered over time to combat viral resistance and minimise toxic side effects (Hammer 2008). Although, life expectancy of infected individuals is increased, the side effects of ARVs can affect the quality of life. This in turn affects the level of compliance to treatment, which requires over 95% compliance for successful treatment (Penedoa 2003). Other limiting factors include viral resistance (which can result in cross-resistance across an entire class of ARVs) and the cost of treatment (Baxter 2006; Reviewed in Stenger 2009). Thus there is a need for a novel HIV treatment option with reduced side effects and which is also cost effective. Aptamers, which are synthetic nucleic acid ligands, are being explored to meet these needs because they represent novel, non-toxic, non-immunogenic molecules that can be directed to bind a variety of targets with great specificity.

1.2. HIV Tropism and Entry

The HIV-1 envelope glycoproteins are produced from a gp160 precursor protein and are targeted by antiviral therapies. The gp160 protein is extensively glycosylated and proteolytically cleaved into two subunits by a cellular convertase (Montagnier 1985; Chan 1997). The cleavage results in gp120, the surface subunit, and gp41, the transmembrane subunit. These subunits remain non-covalently associated as trimers on the surface of the virus (Gallo 2003; Liu 2008). Glycoprotein gp120 was identified to contain variable (V1-V5) regions and four constant regions (C1-C4) (Starcich 1986). The viral envelope glycoproteins mediate viral entry into T lymphocytes and macrophages that express CD4 and chemokine co-receptors (Reviewed by Urchil 2009). Co-receptors CCR5 and CXCR4 are differentially expressed on different CD4+ cells which defines their susceptibility to different HIV-1 strains (Reviewed in Este 2007) (Figure 1).

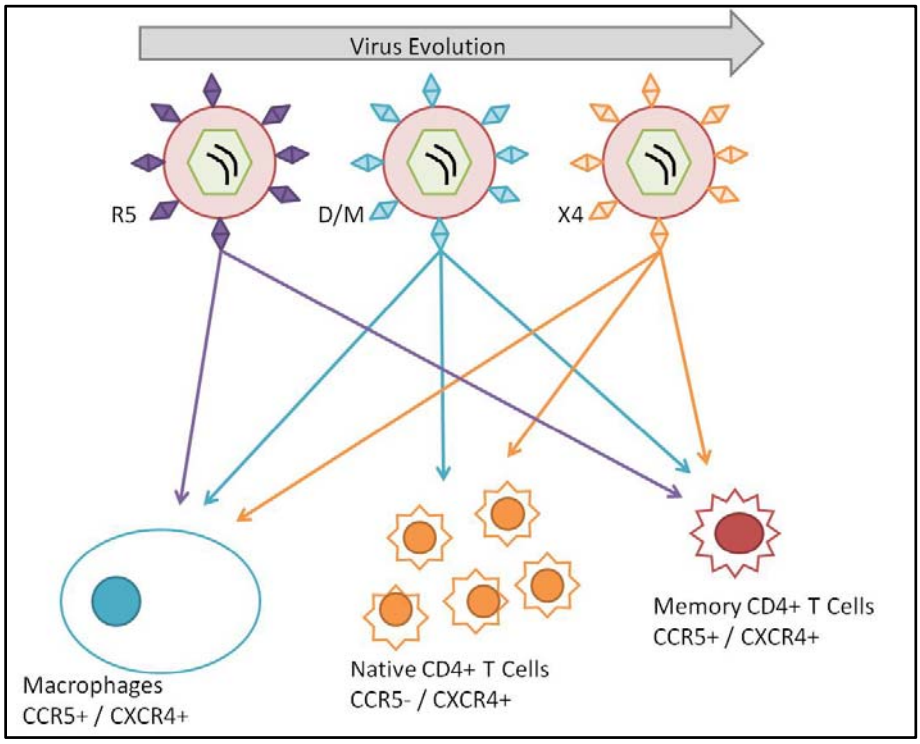


Figure 1: The Progression of HIV-1 Strains and Cellular Tropism.
The choice of co-receptor is determined by the amino acid sequence of gp120. This determines cellular tropism as the co-receptors are not universally expressed. R5 strains use CCR5 as a co-receptor and are associated with acute infection. X4 strains use CXCR4 co-receptor and are associated with disease progression and onset of AIDS. Dual tropic strains (D) can use either co-receptor and show no phenotypic difference to individuals carrying both strains (M). (Adapted from Este 2007)

The use of CCR5 and/or CXCR4 as a co-receptor is dependent on the amino acid sequence within the variable regions V3 and V1-V2 of gp120 (Chan 1999; Pastore 2006). Viral strains making use of different co-receptors have been isolated at different stages of the

disease. R5 strains (making use of CCR5 co-receptor) are preferentially transmitted and are associated with acute infections (Este 2007). X4 strains (making use of CXCR4 co-receptor) however, are associated with increased viral replication, faster disease progression, expanded cell tropism and the onset of AIDS (Reviewed in Biscone 2002; Este 2007). It is still unclear whether a change from R5 to X4 tropism is the cause or consequence of disease progression. Some strains can make use of both co-receptors and are termed dual tropic or R5/X4. Regardless of co-receptor used, HIV entry into human cells requires the following steps in sequence (Reviewed in Gallo 2003; Morris 2005): HIV surface glycoprotein gp120 binds the CD4 receptor on the surface of the host cell; this causes an outward rotation and displacement of each gp120 monomer (Liu 2008) and exposes gp41; gp120 binds a co-receptor, either CCR5 or CXCR4; gp41 penetrates the cell membrane and promotes membrane fusion; finally the viral core enters the cell (Figure 2).

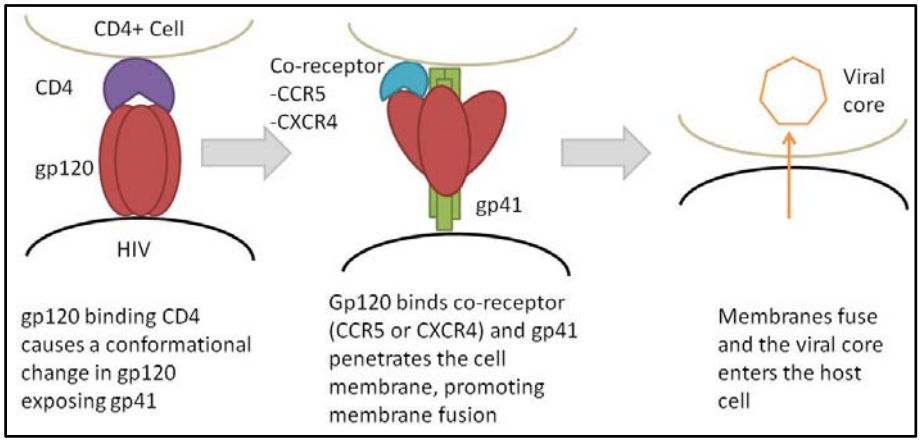


Figure 2: HIV Entry into CD4+ Cells.
Figure illustrates the interaction between viral glycoproteins and cell surface receptors. Special attention is paid to the conformational change seen in gp120 (red) after binding CD4 and the subsequent exposure of gp41 (green). The roles of gp120 and gp41 in the binding of host and viral membranes are shown.

Under native, non-binding conditions, the fusion proteins of gp41 are covered by gp120. This serves to reduce immunogenicity by restricting conserved epitopes from eliciting antibodies. It also reduces antigenicity by preventing elicited antibodies from binding to conserved regions (Zwick 2004). After the attachment of gp120 to CD4, gp41 undergoes a conformational change to a fusion active state that exposes the fusion peptide and N-HR (N terminal portion of the external domain), Figure 3, (Zwick 2004). During this stage, gp41 is most vulnerable but is limited by the short time period required for binding (Frey 2008). The conformational changes of gp41 allow for the insertion of the fusion peptide into the host cell and the generation of a pre-hairpin intermediate (Biscone 2002; Gallo 2003; Zwick 2004).

Once gp120 has dissociated from gp41, it forms a six-helix bundle which promotes membrane fusion (Weissenhorn 1997). The six-helix bundle is formed by the C terminal portion of gp41 (C-HR) and the N-HR in an anti-parallel conformation. This promotes complete fusion of the virus to the host cell and results in the fusion peptide and transmembrane segment of gp41 lying in parallel.

Each protein plays an invaluable role in the fusion of the viral and host membranes. Molecules can be directed towards the glycoproteins or the cellular receptor proteins and inhibit their interaction and the subsequent entry of HIV into CD4+ cells. Treatments that block HIV fusion and entry are termed Entry Inhibitors. Both viral and host proteins involved in membrane fusion are potential targets for antiviral agents.

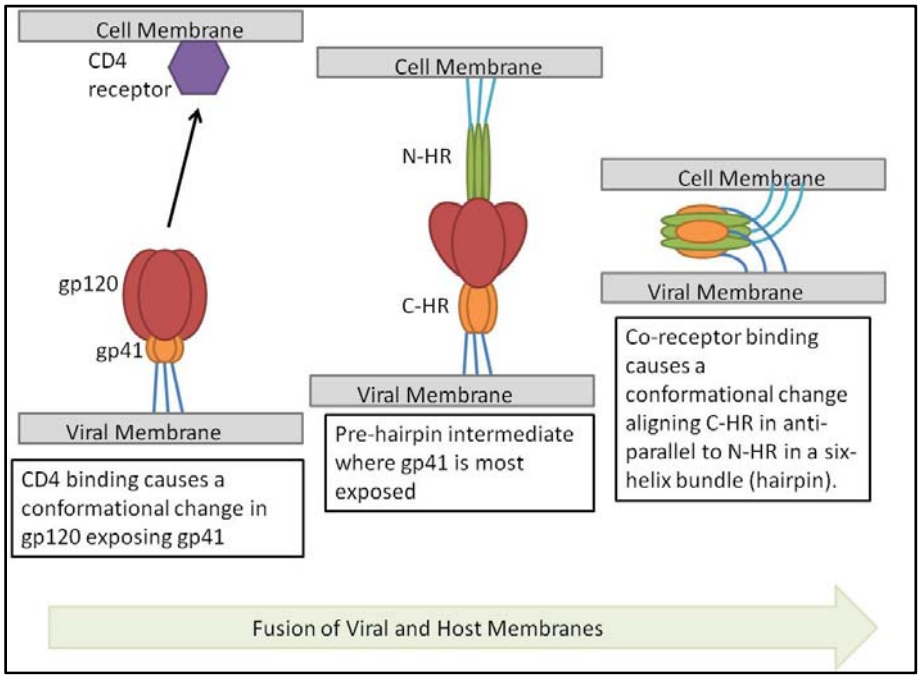


Figure 3: Model of HIV Membrane Fusion.
Under native conditions gp120 and gp41 form a non-covalent association as a trimer. This conformation masks gp41 and in doing so reduces its antigenicity and immunogenicity. Upon binding to CD4, a conformational change in gp120 exposes gp41 (specifically the fusion peptide and N-HR). The N-HR positions the fusion peptide to bind to the host cell membrane. Binding generates a pre-hairpin intermediate in which gp41 is most vulnerable. Conformational changes caused by co-receptor binding align C-HR in anti-parallel to N-HR in a six-helix bundle (hairpin). This process can be inhibited by C-HR peptides. The formation of the hairpin promotes membrane fusion. (Adapted from Chan 1998)

1.3. Entry inhibitors

With the increased knowledge on the entry mechanisms of HIV, each step has been studied in detail to design fusion and entry inhibitors. To date only two entry inhibitors have been approved by the American Food and Drug Administration (FDA). Enfuvirtide also known as Fuzeon or T20, was approved in 2003 making it the first entry inhibitor on the market

(Reviewed in Robertson 2003; Briz 2006). Peptides corresponding to the N-HR and C-HR were found to inhibit HIV-1 entry into cells (Wild 1992; Wild 1994; Reviewed in Zwick 2004). Consequently, T20 and T21 were developed and corresponded to the C-HR and N-HR, respectively. Fuzeon (T20) is directed against gp41 C-HR and prevents the formation of the six-helix bundle. T20 was also found to prevent apoptosis of bystander cells by HIV membrane expressing cells (Meissner 2006). Problems have been noted with Enfuvirtide that correspond to its peptide nature. These include: high production cost, frequent injection site reactions (rarely treatment limiting), relatively short half life, poor distribution in the body, susceptibility to enzyme degradation and rapid renal clearance (Reviewed by Zwick 2004; Este 2007; Jacobs 2008).

In 2007, Selzentry (Maraviroc) was approved and became the first oral entry inhibitor (Flexner 2007). Selzentry is a CCR5 antagonist that prevents co-receptor binding and blocks intracellular calcium redistribution and CCR5 signalling events after chemokine binding (Dorr 2005; Reviewed in Este 2007). Like other CCR5 co-receptor antagonist therapies in development, Selzentry has little to no effect on variant strains that use the CXCR4 co-receptor or have dual tropism (Briz 2006; Flexner 2007). HIV evolves from using CCR5 to CXCR4 co-receptor with progression to AIDS (Biscone 2002). Due to this, the use of a CCR5 antagonist could select for the evolution of X4 strains which, due to their association with disease progression, would not be advantageous (Biscone 2002).

Molecules targeting CXCR4 have been shown to have antiviral activity. Since the first CXCR4 antagonist, a limited number of agents have entered clinical trials, however most have failed (Reviewed in Este 2007). Poor reduction in viral load has been witnessed with the assessment of CXCR4 antagonists and an induced shift from X4 to R5 variants was seen (Este 1999). This highlights the need for a clearer understanding of the tropism switch and co-receptor usage. More recently, AMD11070 was found to be orally bioavailable but clinical trials have since stalled as histological changes in the liver were observed in animal trials (Moyle 2009).

Even though only two entry inhibitors are on the market, many others are in development (Table 1). An overwhelming majority of entry inhibitors in development target the CCR5 co-receptor with only one targeting the virus (Table 1). Bearing in mind the trepidation associated with targeting CCR5 and the possibility that this may cause a co-receptor switch, there is a need for additional treatments with alternative targets.

Table 1: Antiretroviral Drugs in Development During 2009.

Name	Target	Sponsor	Status
Vicriviroc (SCH417690, Schering D)	CCR5 Blocker	Schering	Phase III
TNX-355 (Ibalizumab)	CD4 Blocker (Monoclonal Antibody)	TaiMed	Phase II
PRO 140*	CCR5 Blocker	Progenics	Phase II
INCB9471	CCR5 Blocker	Incyte Corporation	End Phase II[¥]
AK602	CCR5 Blocker	Kumamoto University, Japan	Early Human Trials
AMD070	CXCR4 Blocker	AnorMed	On Hold[§]
BMS-378806[#]	gp120	Bristol-Meyers Squibb	Phase I
GSK 706769	CCR5 Blocker	GlaxoSmithKline	Phase II
HGS004	CCR5 Blocker (Monoclonal Antibody)	Human Genome Sciences	Phase II
PF-232798	CCR5 Blocker	Pfizer	Phase II
SCH532706	CCR5 Blocker	Schering	Phase I
SP01A	CCR5 and CXCR4 Blocker[¤]	Samaritan Pharmaceuticals	Phase III
TBR-652	CCR5 Blocker	Tobira Therapeutics	Phase II
VCH-286	CCR5 Blocker	ViroChem Pharma	Phase II
TAK-652	CCR5 Blocker	Takeda	Phase II

[*] PRO 140 has been granted fast-track status by the FDA
[¥] Incyte Corporation to license INCB9471 to another company for completion
[§] Development on hold due to liver problems in animal studies
[#] BMS-378806 is being investigated for its use as a microbicide for the treatment of HIV subtype B (both CXCR4 and CCR5)
[¤] Reduces intracellular cholesterol and corticosteroid biosynthesis which disrupts the assembly of lipid rafts in cellular membranes
(Taken in part from the *2009 Pipeline Report* by Treatment Action Group (TAG) (www.treatmentactiongroup.org) and Fact Sheet 460 (revised September 2009))

Entry inhibitors being a new class of antiviral therapy may present hope to individuals with HIV strains resistant to other ARVs such as protease and reverse transcriptase inhibitors. Numerous entry inhibitors have been designed, most of which comprised peptides or

antibodies. Aptamers can be developed to bind the glycoproteins involved in HIV entry and fusion. This may provide a novel approach to inhibition of membrane fusion and viral entry.

1.4. Aptamers: A Novel Inhibitory Mechanism

Aptamers are artificial nucleic acid molecules that can be engineered to bind specifically and with high affinity to a particular macromolecule (Reviewed in Ulrich 2006; Yan 2009). Single stranded nucleic acid molecules (RNA and DNA) fold to form complex tertiary structures which interact with cellular proteins and other ligands (Zhang 2004). The selection and design of highly selective aptamers with high affinity to their target has lead to the development of a variety of aptamers capable of binding a multitude of molecules.

The pioneering work, in 1990, by the Gold and Szostak groups (Ellington 1990; Teurk 1990) identified an *in vitro* method for the selection of aptamers specific to organic dyes and T4 DNA polymerases. This method called the systematic evolution of ligands by exponential enrichment (SELEX (Figure 4)) is still in use today and has been adapted to streamline the processes of selection and isolation of aptamers.

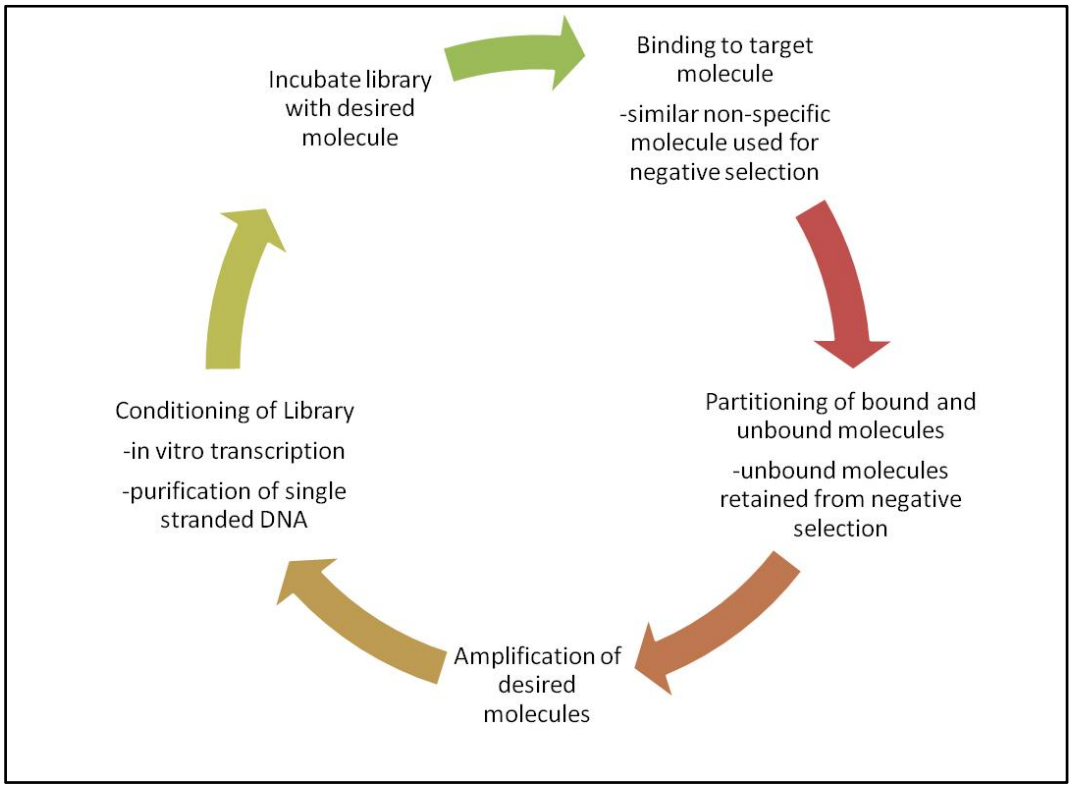


Figure 4: *In vitro* Selection of Aptamers Using SELEX.
A random DNA oligonucleotides library is used for the production of DNA aptamers and can be transcribed into an RNA library. The oligonucleotide library is incubated with the target molecule. The bound oligonucleotides are partitioned from the unbound and partially bound oligonucleotides. This is an essential step for the selection of aptamers with the highest binding affinity. The bound oligonucleotides are eluted and amplified. This is an enriched pool of selected oligonucleotides which is again added to the reaction with the target for further selection. Rounds of selection and amplification proceed until high affinity aptamers are isolated. These can then be used for downstream applications and studies.

SELEX starts with a library of DNA or RNA that is incubated with a target molecule. The bound and unbound molecules are partitioned and the bound molecules are amplified by PCR (Sampson 2003). The library is synthesised chemically with each strand made up of a random region (typically 40 nucleotides) flanked by a fixed sequence (Zhang 2004). The fixed flanking sequences are typically identified by the polymerases used in the process and are invaluable in the selection process. By increasing the random region, the complexity of the library is increased (Zhang 2004) as this allows for increased diversity in the aptamer structures. With a 40 nucleotide random region, the DNA / RNA library can theoretically be composed of 10^{24} distinct molecules with as many different structures.

Cycles of selection and amplification are continued until one or a small pool of aptamers that strongly interact with the protein are selected (Sampson 2003; Yang 2007). A number of non-specific binders can be selected due to non-specific protein interactions and the selection process may not remove all the non bound sequences (this is termed background partitioning) (Djordjevic 2007). For this reason a large number of non-specific sequences can be selected in the first couple of rounds. Thus, a number of selection and amplification cycles are required to reduce the effect of background partitioning on the selection of a high affinity binder.

Many applications of the SELEX method have been developed that attempt to increase selectivity while decreasing selection time (Djordjevic 2007; Stoltenburg 2007; Yang 2007; Wei 2009). The chemical synthesis of aptamers results in little to no batch variation (O'Sullivan 2002). This is a great advantage of aptamer technology for therapeutic application as it implies an inherent quality standard that is not matched by other molecules.

1.4.1. *Aptamers vs. Antibodies*

Due to the severity of HIV as a global health problem, there is investigation into numerous types of prevention and treatment. Entry inhibitors have been identified as a potential strategy, not only as a treatment but as prophylactic as well. The potential of antibodies for this has been widely investigated. During the course of HIV infection, antibodies are raised against epitopes on gp120 (Stamatatos 2009). These are generally not conserved and lead to transient inhibition before the generation of escape mutants (Kelker 2010). It has been identified that to develop a successful antibody based vaccine for HIV it must encompass both broadly neutralising antibodies (NAbs) and an HIV specific T cell response (Phogat 2007). Due to their immunogenic properties and involvement in HIV entry, the surface glycoproteins are a major target for the development of NAbs. NAbs have been developed to

a variety of HIV epitopes with varied success (Zwick 2001; Gorny 2002; Raja 2003; Mello 2005; Miller 2005). NAbs represent a possible vaccination option, however, their use is not without problems.

Aptamers have advantages over their antibody counterparts on a number of levels. Preparation of aptamers is faster and simpler than that of antibodies which would allow for easier scale up of production. Aptamers have the same or higher affinity with their targets than antibodies and usually show dissociation constants ranging from low picomolar to low nanomolar (O'Sullivan 2002; Zhang 2004). Strong binding affinity to a target molecule is essential if an aptamer is to be used for efficient and effective drug delivery. Binding affinity represented by the dissociation constant provides information regarding binding strength and stability of two molecules. The lower the dissociation constant, the tighter the binding and the less the molecules tend towards being apart**.** Thus, the best candidate for pharmaceutical application would have a low dissociation constant and a high specificity to the target. In a contrasting theoretical study by Eaton et al (1995) suggested that a tight and specific binding aptamer may be affected more readily by mutations within the binding site. A strong binding affinity within a very small region may be more susceptible to minor changes in amino acid sequence or protein conformation and thus may not be the best candidate (Eaton 1995). Although these conclusions have been refuted by the identification of aptamers that can neutralise more than one strain of HIV (by binding to gp120) it is worth noting.

Aptamers have been shown to be able to discriminate between targets with subtle structural differences such as isoforms of a protein (Jenison 1994; Gopinath 2006). This is an invaluable characteristic when dealing with a pharmaceutical as it would enable the aptamer to distinguish between healthy and disease cells even when the difference is minor. As testament to their high binding specificity, aptamers have been selected for use in affinity chromatography as affinity ligands (Hage 1999). By making use of this characteristic, biomarkers for disease conditions have been identified using aptamers. Aptamer-facilitated biomarker discovery (AptaBiD) has been shown to overcome the major problems previously encountered with biomarker discovery such as false positives and false negatives due to sample processing and differences in localisation and modification of proteins (Berezovski 2008). Berezovski et al (2008) successfully identified biomarkers for immature and mature dentritic cells. They went further to highlight how the aptamers used could have far reaching applications including targeted delivery of therapeutics, cell visualisation, tracking cells *in vivo* and as drug candidates themselves.

Aptamers can be selected to bind a wide range of macromolecules including those that have low immunogenicity or are toxic substances (O'Sullivan 2002; Wei 2009). Antibodies are limited by the immunogenicity of their targets. However a recent publication highlighted a method for eliciting antibodies to conserved and non immunogenic epitopes with the aid of multi copy proteins (MCP) (Kelker 2010). Aptamers are more stable than antibodies and can be stored long term at ambient temperature (Wei 2009). Denatured aptamers can be regenerated while antibodies have a short life span and cannot be regenerated after denaturation. Aptamers are able to discriminate between targets based on subtle structural changes such as the presence or absence of a methyl or hydroxyl group (O'Sullivan 2002). Due to their high specificity, aptamers can be directed against highly specific targets. This has been applied to a wide range of therapeutics, specifically for cancer treatment. Aptamers can be used to transport inhibitory molecules to specific cells reducing the off target effects seen in current treatment. Studies have looked at chemically binding or co-synthesising aptamers and siRNA so that they can be selectively targeted to cells expressing relevant receptors (Reviewed in Castanotto 2009).

1.4.2. *Current and Future Prospects of Aptamer Technology*

Aptamer research encompasses a wide range of fields. Their high specificity and small size makes them ideal for use in analytical, therapeutic and diagnostic applications. Aptamers have been developed against various HIV components including: gp120 (Khati 2003), Integrase (de Soultrait 2002), Reverse-Transcriptase (Andreola 2001) and the *trans*-activation response (TAR) RNA (Duconge 1999). Aptamers have also been raised against drug resistant strains of HIV in an attempt to overcome challenges associated with drug resistance (Li 2008). There is potential for aptamer mediated treatment of HIV at many levels. When targeting gp120, aptamers can be designed for use as entry inhibitors. A major challenge when working with gp120 is its probable unstable conformation and the large conformational change seen when gp120 binds CD4 (Kelker 2010). In addition, gp120 is mostly shielded from immune response by a cover of negatively charged carbohydrate groups (Sayer 2002). These inhibit the binding of molecules not only by reducing immunogenicity but by steric hindrance of immunogenic epitopes on the gp120 molecule. Aptamers are small enough to not be affected by steric hindrance of the gp120 molecule increasing the epitopes available to them. By identifying the minimal sequence required for its binding, an aptamer can be reduced in size to contain only the essential binding sequence (Dey 2005). This would further limit the effects of steric hindrance against aptamer binding.

A range of aptamers have been developed that bind within the CCR5 binding region of the gp120 molecule and effectively block HIV binding to the cell surface (Sayer 2002; Khati 2003; Dey 2005; Cohen 2008). Specific examples of such aptamers are those described by Khati et al (2003) that were selected for their ability to bind gp120 of HIV-$1_{Ba\text{-}L.}$ Some of the aptamers selected were found to bind within the conserved CCR5 binding region of gp120 and neutralise HIV infectivity. HIV-$1_{Ba\text{-}L}$ is a subtype B virus that is not prominent outside of the Americas, Europe and Australasia and so further study included neutralisation test on other variants in which some aptamers were successful (Khati 2003). One aptamer highlighted by Khati (2003), B40, has subsequently been highly characterised and tested against other strains of HIV. A synthesised version of the B40 aptamer is now commercially available for laboratory use as UCLA (Cohen 2008).

Some of the aptamers used in this study were identified in the same study as B40 but have not been as highly characterised. These aptamers were raised against monomeric gp120 which is not its natural state. The other set of aptamers used in this study were raised against HIV-1_{CAP45} (a subtype C virus) pseudovirus expressing the whole glycoprotein complex. This is a better representation of the gp120 encountered if used as a therapeutic agent. Both sets of aptamers were tested on a subtype C gp120 as subtype C is the most predominant subtype. In 2004, subtype C HIV was responsible for more than 50% of all infections worldwide (Hemelaar J. 2006). Aptamers may provide a novel treatment for HIV infection and rival the numerous antiviral therapies currently available as well as those in development.

To date, only one aptamer based therapeutic has been approved by the FDA and is on the market. In 2004, Macugen (Pegaptanib) was approved to slow vision loss due to all subtypes of neovascular age-related macular degeneration (AMD) (Gragoudas 2004; Nowak 2006). Previous studies identified angiogenesis as the underlying cause of AMD which is regulated by many factors and isoforms (Eugene 2005). Macugen targets $VEGF_{165}$ (vascular endothelial growth factor) and successfully treats AMD by targeting the underlying cause (Gragoudas 2004).

For future aptamer mediated therapies a number of obstacles must be considered. A key problem facing the use of aptamers *in vivo* is their rapid degradation and clearance from the body. Within biological fluids, aptamers are susceptible to nuclease degradation rendering them ineffective. Although many of the solutions to nuclease degradation were provided over 10 years ago, it still comes up as an important consideration in aptamer design. The numerous methods identified to circumvent this problem make use of the fact that nuclease activity relies on the ribose 2′-OH group and modification of this can significantly decrease nuclease

activity (Zhang 2004). However, modification of the aptamer 2′ end must take into consideration the enzymes used in SELEX and must not disrupt their functioning. Modifications such as adding an amino (NH_2), fluoro (F) or 2′-*O*-alkyl group to the 2′ end do not interfere with the SELEX enzymes and increase nuclease resistance by as much as 1000-fold (Osborne 1997; Zhang 2004). Other modifications such as adding a benzoyl group at the C5 position, using phosphorothioated oligonucleotides and replacing D-ribose with L-ribose (Spiegelmers method) and using locked nucleic acids in aptamer design (Darfeuille 2004) have shown to increase nuclease resistance (Zhang 2004). Most recently the production of a circular RNA aptamer was reported by Umekage and Kikuchi. This aptamer not only retained its binding properties after purification but avoided exonuclease-induced degradation *in vivo* and *in vitro* increasing the half life by 30 -fold (Umekage 2009). This method eliminates the need for 2′ modifications which can affect ligand specific binding ability (Umekage 2009). Although this method protects the aptamer against exonuclease mediated degradation, the circular aptamers were degraded in human sera. This was attributed to RNase A-like activity (although the precise causative agent is still unknown) (Umekage 2009). Although not flawless, this method of production created new options for aptamer design. With the availability of many techniques for reduced susceptibility, one can focus more on the problems of bioavailability and delivery of aptamer therapeutics. Currently aptamer based therapies are delivered via injection; there is hope that future technology may allow for oral or dermal application.

Another setback of aptamer therapy is its bioavailability. Aptamers, ranging from 8-15 kDa, are roughly one tenth the size of antibodies (155 kDa) (Zhang 2004). With such small size, aptamers are rapidly removed from the blood and cleared from the body (Zhang 2004) thus reducing bioavailability. To circumvent this, aptamers are conjugated to high molecular weight molecules such as polyethylene glycol (PEG), streptavidin or to the surface of liposomes or nanoparticles (James 2001; Zhang 2004). This problem highlights the importance of adequate kinetic analysis of potential aptamers. The aptamers identified by Khati (2003) were identified with numerous applications in mind. One of which was for them to act as entry inhibitors for HIV-1 as they bind to gp120 and thus inhibit binding of HIV to target cells. For this application to be successful, the aptamer would have to bind to the gp120 molecule with great affinity and have a low dissociation constant. The aptamer that has a sufficiently low dissociation constant and sufficiently high target affinity would bind the target molecule quickly and for long enough to increase bioavailability. Kinetic data could

then be used for the selection of aptamers with the potential for downstream applications such as a carrier and / or targeting molecule.

1.4.3. *Application of Aptamer Technology: Delivery of siRNA*

An aptamer that binds gp120 with high affinity would open the door for numerous therapeutic applications such as: directly inhibiting HIV-1 entry or transporting other inhibitory molecules (Cohen 2008; Xiao 2008). Aptamers have been previously used as targeting molecules for cancer treatment, this technology has application in numerous diseases (Dhar 2008). Another example is the use of aptamers to transport and deposit siRNA, capable of inhibiting the HIV, into an infected cell (Zhou 2009). In this way, cells that have been previously infected by HIV can be selectively targeted by the RNA interference (RNAi) therapy.

RNAi is a conserved gene silencing pathway that makes use of a double stranded RNA trigger and a range of cleavage and recognition proteins (Saayman 2008; reviewed by Siomi 2009). This gene silencing pathway has been exploited for the generation of numerous therapeutics suppressing viral genes or rouge cellular genes (reviewed in Boutros 2008). RNAi is an ATP-dependent and transcription-independent mechanism of gene silencing that occurs post transcriptionally in the cytoplasm (Chen 2008).

Genes can be silenced by degradation of mRNA inhibiting the production of the gene product. This is mediated in a homology dependent manner by siRNA, a 9-24 base pair double stranded RNA molecule with a two nucleotide 3′ overhang (Chen 2008). Briefly, the RNAi machinery recognises the siRNA by its overhang and cleaves it. The short double stranded RNA molecules generated by cleavage, directs the degradation of mRNA molecules that are of perfect or near-perfect homology (Chen 2008). Constanotto (2009) provides a clear overview of the mechanisms of gene silencing by siRNA. siRNA has been used in therapies for a wide range of diseases and infections, some of which include: hepatitis B and C virus (Arbuthnot 2007; Chen 2008), neurodegenerative disorders (Weinberg 2009) and HIV (Cave 2006; Barichievy 2007). By coupling the direct targeting of aptamers with the strong inhibitory effect of siRNA, a promising anti-HIV treatment could be developed.

1.5. Problem Identification

Prior to any downstream applications, a sound knowledge of the aptamer binding kinetics is essential. It is for this reason that this project determined gp120 binding kinetics for a group of aptamers previously identified by Khati (2003) and a group of aptamers raised against trimeric HIV-1_{CAP45} gp120 (Grace London, unpublished data). Much like B40, these

aptamers too could represent good candidates for therapeutic applications. The kinetic analysis of this project will aid in the identification of these molecules as possible leads.

1.6. Research Objectives

The primary objective of this study was to characterise selected aptamers and determine their binding kinetics to subtype C gp120.

Secondary objectives were:

1. **To *in vitro* transcribe a selected number of monoclonal aptamers isolated against monomeric HIV-$1_{Ba\text{-}L}$ gp120 and HIV-1_{CAP45} Env pseudovirus, respectively**

2. **To screen these aptamers for binding to HIV-1_{DU151} and HIV-1_{CAP45} monomeric gp120 and determine their kinetics**

3. **To determine the secondary structure of the selected aptamers**

2 Methods

2.1. Cell Maintenance

293T mammalian cells (Invitrogen) were seeded at a density of 5×10^5 cells/ml. The cells were maintained in 15 ml Dulbecco's Modified Eagle's Medium (DMEM), 10% Foetal Calf Serum (FCS), 50 mg/L gentamicin, 0.25% 4-(2-hydroxyethyl)-1-piperazineethanesulfonic acid (HEPES)) in a humidified incubator with 5% CO_2 at 37 °C.

2.2. Selection of Aptamers

The aptamers used in this research were raised against two different proteins. One set, (B19, B11, B65, B5 and B84) identified by Khati (2003) were raised against monomeric gp120 from a subtype B virus called HIV-$1_{Ba\text{-}L}$. The other set (P2, P10 and T58) were isolated against whole subtype C HIV-1_{CAP45} pseudotype virus (Grace London, unpublished data). UCLA, which is a shortened synthetic derivative of the B40 aptamer, was used for comparison and as a positive control.

B19 was selected because it neutralises HIV-$1_{Ba\text{-}L}$ but does not bind within the CD4 epitope of gp120. B65 is very short and neutralises HIV-$1_{Ba\text{-}L}$. B84 and B11 were shown to be very strong neutralisers of HIV-$1_{Ba\text{-}L}$. B5 was shown not to neutralise HIV-$1_{Ba\text{-}L}$ but was included to compare the binding kinetics with the good neutralising aptamers. Since monomeric gp120 is not present on native HIV aptamers selected against trimeric gp120 were chosen because they were expected to show better binding and neutralisation of the virus. P2, P10 and T58 aptamers were selected for binding to the whole CAP45 glycoprotein (including gp120 trimer and gp41). All these aptamers bind gp120 CAP45 and neutralised HIV-1_{CAP45} (Grace London, unpublished data). These aptamers were selected for kinetic analysis due to their strong binding and neutralisation properties.

2.3. Oligonucleotides

The aptamers used in this research were generated by *in vitro* transcription of the Polymerase Chain Reaction (PCR) product from the plasmid DNA. Each aptamer is made up of the same T7 and T3 SELEX primers flanking randomized nucleotides. This allows for aptamers with different binding properties and structural characteristics from within the same pool. The aptamers sequences can be seen in the table below (listed $5' \rightarrow 3'$).

Table 2: Nucleotide Sequences of the Common Flanking Regions (T7 and T3) and Random Internal Regions of the Selected Aptamers.

Sequence name	Sequence
T7 SELEX primer	**TAATACGACTCACTATA**GGGAGACAAGACUAGACGCUCAA
T3 SELEX primer	UUGACAUGAGACUCACAACAGUUCCCUUUAGUGAGGGUUAAUU
B19	AGACCUUAUACCUGAGAUUACACGCUCUUCGAGCACGUCGAC
B65	GAACACCAUCGG
B84	AUGACGUACCCGCACAAGCCACCACAAGUCUUAAUCGCGCCACCCUUGC
B5	GGGCGCUUAAUGUAUGCCGUAUGACCCUCAACAUCCGACUCAGUUAAGC
B11	CCAAGGGCUAAGUCCGCAAAUAUCCUUCCUAAAGGACUCGUUACGUCGG
P10	AGUAGUCGAUGGGAUUGCUAGGCCGGUCAUCAUGAAAACGAAGUCGA
T58	CAAAUCAUUUCCAAUAAGGGGAGUACUAAGAGGCCAUUCAAAAAACGAAA
P2	AUUUGAAGUCGGUGGCAAGAUGGUGCGCUCAUGAAGGCAUCUUCGG

***** T7 SELEX primer includes the T7 promoter sequence which is not transcribed; this is seen in bold and underlined (the promoter sequence is in DNA however, the remaining sequence is displayed as transcribed RNA).

2.4. Polymerase Chain Reaction

Plasmid DNA of each aptamer had to be amplified before *in vitro* transcription; this was achieved using polymerase chain reaction (PCR). Each 100 µl reaction mixture contained 1 × Taq buffer (Promega), 1 mM $MgCl_2$ (Promega), 0.2 mM dNTPs (Fermentas), 1 µM T3 and T7 primer (Inqaba Biotech), 1 U Go Taq Polymerase (Promega) and 100 ng DNA. A twenty eight cycle PCR was performed with the following parameters: 93 °C for 30 seconds for denaturation, 72 °C for 1 minute for annealing and 72 °C for 8 minutes for extension.

The PCR product was cleaned by centrifugation using a PCR purification kit (Promega Wizard). PCR product was prepared for clean up by adding equal volume Membrane Binding Solution. One SV mini-column was placed in a Collection Tube for each PCR product to which the PCR product-Membrane Binding Solution was added and incubated for 1 minute. The SV mini-column assembly was centrifuged at 16 000 × *g* for one minute after which the liquid in the collection tube was discarded. The SV mini-column was returned to the collection tube and was washed with 700 µl Membrane Wash Solution (previously diluted with 95% Ethanol). The SV mini-column assembly was again centrifuged at 16 000 × *g* for 1 minute. The collection tube was emptied and the SV mini-column was returned. The wash was repeated with 500 µl of Membrane Wash Solution and centrifuged at

16 000 × *g* for 5 minutes. The collection tube was again emptied and the SV mini-column returned. The assembly was centrifuged at 16 000 × *g* for 1 minute to evaporate remaining ethanol. The SV mini-column was then transferred to a 1.5 ml microfuge tube and 50 µl nuclease-free water was added to the centre of the column. The assembly was incubated at room temperature for 1 minute before centrifugation at 16 000 × *g* for 1 minute. The microfuge tube then contained the purified DNA and the SV mini-column was discarded.

DNA quantification was obtained using a NanoDrop-spectrophotometer at A_{260}. Fractions of the clean DNA were resolved on a 2.5% agarose gel (containing 5% Ethidium Bromide) in 1 × TBE running buffer. The DNA was visualised under UV light. A Mass Ruler Low Range DNA Ladder (Fermentas) was used for DNA sizing and quantification by Molecular Imager Chemidoc XRS+ Imaging System (BIORAD). DNA was retained for RNA aptamer production by *in vitro* transcription.

2.5. *In vitro* Transcription

In vitro transcription was done as previously described (Khati et al. 2003). Briefly, 100 µl reaction mixtures contained: 1.5 ng DNA, 1 × transcription buffer (New England Biolabs, 40 mM Tris-HCl, 6 mM $MgCl_2$, 10 mM Dithiothreitol, 2 mM spermidine), 2 mM spermidine, 1 mM rATP, 1 mM rGTP, 1.5 mM 2′F CTP, 1.5 mM 2′F UTP (Fermentas), 2 U T7 RNA Polymerase (New England Biolabs). Transcription reaction was incubated overnight at 37 °C.

Transcription was stopped with the addition of 1 U RNAse free DNAse I in 1 × Reaction Buffer (Fermentas, 100 mM Tris-HCl (pH 7.5 at 25°C), 25 mM $MgCl_2$, 1 mM $CaCl_2$) and incubated at 37 °C for 25 minutes. RNA was purified from low molecular weight contaminants on a 0.9 G50 column. The G50 column is made up of a 1 ml pipette tube loaded with Sephadex solution (6.5 % sephadex (w/v) suspended in 0.02% NaN_3) and washed with 150 mM NaCl. The transcription solution was incubated with 1% Phenol Red solution before being loaded to the column. Phenol red stains the free nucleotides which are retarded by the sephadex beads. The full length RNA was eluted first in a clear solution by the addition of 600 µl 150 mM NaCl. This significantly reduces the concentration of the RNA in solution and thus RNA must be precipitated out.

Purified RNA was precipitated in 5:1 phenol-chloroform-isoamyl alcohol pH 4.7 and extracted with chloroform. The extract was incubated at -80 °C for 2 hours in 0.1 Vol 3 M NaAc pH 5.2 and 1 Vol Isopropanol. After incubation, it was centrifuged at 4 °C for 30 minutes (190 × *g*). Supernatant was discarded and the pellet washed with 70% Ethanol.

Ethanol was removed and RNA was re-suspended in 50 µl nuclease-free water (Fermentas). RNA was quantified by spectrophotometry at A_{260}. RNA fractions from each step were resolved on a 12% denaturing (8 M Urea) polyacrylamide gel (pre-run for 30 minutes at 200 V), with 1 × TBE running buffer at 200 V for 45 minutes, to validate the process. Prior to running on a denaturing PAGE gel, RNA was incubated with 2 × RNA loading dye (95% formamide, 0.025% SDS, 0.025% bromophenol blue, 0.025% xylene cyanol FF, 0.025% ethidium bromide, 0.5 mM EDTA, Fermenas) and heated to 70 °C for 15 minutes. Visualisation was achieved under UV light by 0.1% (v/v) Ethidium Bromide staining.

For the correct folding, aptamers were denatured at 95 °C for 4 minutes (incubated at room temperature for 4 minutes), refolded in the presence of 1 × HMKCN buffer (10 mM Hepes pH 7.4, 1 mM $MgCl_2$, 1 mM $CaCl_2$, 2.7 mM KCl, and 150 mM NaCl) and incubated at room temperature for 10 minutes prior to use.

2.6. Expression of gp120

HIV-1_{DU151} envelope glycoprotein gp120 was expressed and purified in 293T mammalian cell line, using lipofection (Felgner 1987) to transfect the plasmid. Transfection followed the manufacturer's protocol for FuGENE 6 Transfection Reagent (Roche). Briefly, 293T cells were seeded at a concentration of 1 × 10^6 cells/ml in a hyper flask in 50 ml $DMEM^{10}$ (dulbecco's modified eagle's medium, Invitrogen) (10% Foetal calf serum (Invitrogen), 2.6% HEPES (Invitrogen), 0.5% Gentomycin (Invitrogen)) and incubated at 37 °C in a humidified incubator with 5 % CO_2 overnight. Transfection mixture (72 µl FuGENE, 25 µg DNA 15 ml serum free DMEM) was added to cells at 50% confluency. The transfection was incubated at 37 °C in a humidified incubator with 5 % CO_2 for 48 hours. Supernatant was harvested every 48 hours until the monolayer of cells started to detach from the flask surface. Culture supernatant was centrifuged at 3900 × *g* for 10 minutes, filter sterilised through a 0.45 micron filter and stored at – 20 °C.

2.7. Sodium Dodecyl Sulphate Polyacrylamide Gel Electrophoresis

The presence and purity of the desired protein was confirmed using sodium dodecyl sulphate polyacrylamide gel electrophoresis (SDS-PAGE). Transfection supernatant was incubated with SDS-PAGE sample buffer (0.125 M Tris-HCl, 4% (w/v) SDS, 20% (v/v) glycerol, 5% (v/v) β-mercaptoethanol and 0.02% (w/v) bromophenol blue, pH 6.8) for 5 minutes at 95 °C.

These samples were resolved on an 8% SDS-PAGE gel at 150 V in 1× SDS-PAGE running buffer (25 mM Tris-HCl, 200 mM Glycine, 0.1% (w/v) SDS) to identify the presence of the desired protein. Full Range rainbow protein molecular weight marker (AEC-Amersham) was used as a standard. The gel was stained using coomassie Stain (40% methanol; 0.7% acetic acid; 0.075% coomassie dye) and destained with coomassie destain (40% methanol; 0.7% acetic acid). Purified protein was used for binding and kinetic experiments.

2.8. Western Blot

A western blot was used to confirm the protein presence. Protein was transferred to the nitrocellulose membrane at 4 °C overnight at 30 V in 1 × transfer buffer (50 mM Tris, 380 mM glycine, 0.1% (w/v) SDS, 10% (v/v) methanol pH 8.3). After transfer to the nitrocellulose membrane, the membrane was blocked with 5% fat free powder milk in phosphate buffered saline, PBS, (1M KH_2PO_4, 1M K_2HPO_4, 5M NaCl in 1*l*) (Sigma-Aldrich) for 1 hour. After blocking, the membrane was probed with the 1:20 000 dilution of human serum from HIV-1 positive patients containing a high level of anti-HIV-1 gp120 antibodies in 2.5% (w/v) fat free milk powder in PBS.

After incubation with the primary antibody solution, the membrane was washed in 0.05% PBS Tween-20 (0.01 M phosphate buffer, 0.0027 M KCl, 0.14 M NaCl, 0.05% Tween, pH 7.4 in 500 ml) (Sigma-Aldrich) solution three times for 10 minutes. The 0.05% PBS Tween-20 was removed and the membrane was incubated with 5% blocking buffer for 1 hour. Blocking buffer was discarded and the membrane was incubated with the secondary antibody (goat-anti human 1: 20 000) (Kirkegaard & Perry Laboratories, Inc.) for 1 hour. Secondary antibody solution was discarded and the membrane was washed with 0.05% PBS Tween-20 three times for 10 minutes. The immunereactive bands were detected using an enhanced chemiluminescence detection system (Amersham Pharmacia Biotech) according to manufacturer's protocol. A purified HIV-1_{ConC} gp120 protein was included as a positive control.

2.10. BIAcore Surface Plasmon Resonance Assays

BIAcore 3000 (BIAcore AB Inc.) SPR assay, was used to determine the binding capacity and kinetics of each aptamer to gp120 and to ensure the correct structural conformation of bound gp120. Research grade CM5 chips, EDC (1-Ethyl-3-(3-dimethylaminopropyl) carbindiimide

hydrochloride), NHS (N-Hydroxysuccinimide), Ethanolamine and HBS-N running buffer used in all the SPR experiments were obtained from BIAcore AB Inc. For the preparation of CM5 chips, 1 × HBS-N buffer (10 mM Hepes, 150 mM NaCl, pH 7.4) running buffer was injected at a flow rate of 10 µl/min. CM5 sensor chips were activated with 0.2 M EDC and 0.5 M NHS for 10 minutes. By amine coupling chemistry 20 000 response units (RU) gp120 at 25 µg/ml (buffer exchanged in 10 mM NaAc) was immobilised to the experimental flow cell(s). A flow cell with no protein bound was included as a negative control. This allowed for the deduction of non-specific background binding during analysis. After protein immobilisation, remaining activated carboxymethyl groups were blocked by flowing 1 M Ethanolamine for 7 minutes. Non-specifically bound protein was removed with 10 mM Glycine-HCl injected for 3 minutes. Resultant sensorgrams were analysed using BIAevaluation 4.1 software (BIAcore AB Inc.). The negative control was either deducted from the experimental result to correct for non-specific binding or was included in the graphs as a point of reference.

2.10.1. Validation of Protein Structure

Monoclonal antibody b12 binding was used to determine if the protein produced was bound to the CM5 chips (for use on the BIAcore 3000, BIAcore AB Inc.) maintained the correct confirmation. The CM5 chip was prepared as indicated above (Section 2.10) with one experimental and one control flow cell. IgGb12 antibody (14 µg/ ml in 10 mM NaAc pH 5.0) was injected over the two flow cells for 5 minutes at a rate of 10 µl/ minute. The chip was regenerated with 20 nM NaOH injected for 1 minute. BIAevaluation software (BIAcore AB Inc.) was used to evaluate the binding of b12 monoclonal antibody to the protein. The negative flow cell results were deducted from the experimental results to adjust for non-specific binding and instrument noise.

2.10.2. Aptamer Binding to gp120

Binding was assessed with 200 nM aptamers to 20 000 RU gp120. Aptamers were denatured at 95 °C for 4 minutes and refolded using 1 × HMCKN buffer (10 mM Hepes pH 7.4, 1 mM $MgCl_2$, 1 mM $CaCl_2$, 2.7 mM KCl, 150 mM NaCl). Aptamers were incubated at room temperature for 6 minutes prior injection to ensure correct refolding. Each aptamer was injected for 3 minutes at 10 µl/ minute. The chip was regenerated after injecting each aptamer with 20 nM NaOH injected for 1 minute.

2.10.3. Aptamer Binding Kinetics on gp120

The binding kinetics of aptamers was determined using monomeric gp120. The level of protein immobilised was optimised using 23 000 RU, 13 000 RU and 3000 RU of immobilised gp120 on three flow cells. A fourth flow cell with no protein immobilised was included as a negative control. Optimisation preceded experimentation as kinetics analysis requires a dose-dependent binding assay to determine mass transport limitations on kinetics. For the kinetic experiment 25 µg/ml gp120 was injected over three flow cells for 3 minutes at a flow rate of 10 µl/ minute. The three experimental flow cells served as triplicate kinetic analyses essential for the determination of a standard deviation of kinetic analysis.

Aptamers were denatured at 95 °C for 4 minutes and refolded using 1 × HMCKN buffer (10 mM Hepes pH 7.4, 1 mM $MgCl_2$, 1 mM $CaCl_2$, 2.7 mM KCl, 150 mM NaCl). Aptamers were incubated at room temperature for 6 minutes before injection. Aptamers were injected at 70 µl/ minute in ascending concentration order (from 4.5 nM to 300 nM). The aptamers were injected using KINJECT with the dissociation time set to 600 seconds allowing for a contact time of 43 seconds. The chip was regenerated after each aptamer injection with 20 nM NaOH which removed the bound aptamer.

Aptamer association rates (k(on)), dissociation rates (k(off)) and dissociation constants (K_d) were calculated with BIAevaluation 4.1 software (BIAcore AB Inc.) The goodness of fit was calculated based on an agreement between experimental data and calculated fits and was expressed as a Chi^2 value less than 1. The kinetic parameters were analysed using the 1:1 Langmuir binding model initially calculated with the simultaneous ka / kd analysis tool and later with the separate ka / kd analysis tool. The separate ka / kd tool allowed the user more control over the analysis and produced more statistically relevant data (i.e. Chi square values were systematically closer to 1) although the resultant K_d in both cases were similar. The result for the empty flow cell was subtracted from the experimental flow cells to correct for refractive index changes due to non-specific associations and instrument noise. Kinetics on each flow cell individually was analysed individually. The results were examined together to produce a standard deviation for the calculated K_d.

2.11. Computational Analysis of Aptamer Secondary Structure

MFOLD (http://mfold.bioinfo.rpi.edu/) was used to computationally identify secondary structures possible within the aptamer using the sequence information (Zuker 2003). The nucleotide sequences were added in FASTA format as linear RNA molecules. Secondary

structure predictions were made at 37 °C with no divalent ions, 1M NaCl, 5% suboptimality, an upper limit of 50 computed folding, a maximum interior / bulge loop size of 30 bp and maximum asymmetry of interior / bulge loop of 30 bp. No limit was defined for the distance between base pairs and *pnum* values were included in the analysis outputs. A *pnum* value is assigned to each base in a structure and provides certainty for the prediction by indicating the number of different conformations that contain the same feature.

3 Results

3.1. PCR of Aptamer Clones

Aptamer clones were amplified by PCR to generate enough DNA for *in vitro* transcription. The amplified PCR product contained a T7 promoter sequence necessary for the transcription reaction that was introduced by the forward primer. The T7 promoter sequence was required for the activation of bacterial T7 polymerase, a DNA dependent RNA polymerase responsible for the conversion of the PCR product (DNA) to RNA aptamers.

After PCR the DNA was resolved on a 2.5% agarose gel to verify the quality and visually quantify the DNA (Figure 5). The amplified sequences were expected to correspond to the number of bases shown in Table 3. Aptamer length varied according to the number of nucleotides incorporated into the variable region as the size of the flanking regions was consistent between aptamers.

Table 3: Aptamer Sizes in Number of Bases

Aptamer Name	Number of Bases	Aptamer Name	Number of Bases
B19	108	**B5**	115
B65	78	**P2**	112
B84	115	**T58**	116
B11	115	**P10**	113

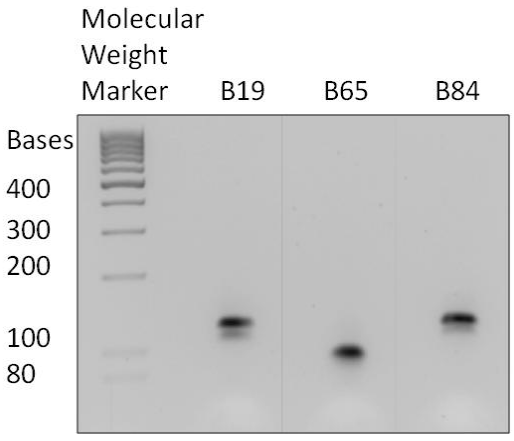


Figure 5: 2.5% Agarose Gel of Representative PCR Products Used for Transcription.
B19, B65 and B84 fragment sizes were determined using the molecular weight marker and corresponded to the expected fragment size.

Amplified DNA for aptamers B19, B65 and B84 resolved on a 2.5% agarose gel corresponded with the expected size of the aptamers (Figure 5 and Table 3). Artefacts on the gel could be due to incomplete amplification of the DNA (Figure 5). The correct sized band contained more DNA indicated by the relative brightness of the band. It was concluded that possible incomplete amplification would not compete with fully amplified stands during the transcription reaction due to their relative concentrations.

3.2. *In vitro* Transcription of Aptamers

To convert amplified DNA clones into RNA aptamers *in vitro* transcription was used. The DNA clones included a promoter sequence for a bacterial T7 polymerase. This DNA dependent RNA polymerase was responsible for the conversion of the PCR product (DNA) to RNA aptamers. During the *in vitro* transcription reaction fluoropyrimidines (cytosine and uracil) were incorporated into the aptamer structure to protect the RNA from nuclease degradation and make the RNA more stable.

Denaturing PAGE of reaction aliquots from the transcription of B84 indicated that the transcription reaction had been successful (Figure 6). Denaturing PAGE shows high molecular weight RNA bands of the correct size indicating that correct sized fragment was transcribed (Figure 6). However, low molecular weight bands are seen in all reactions indicating that there may have been partial degradation of some DNA prior to transcription resulting in smaller fragments (Figure 6).

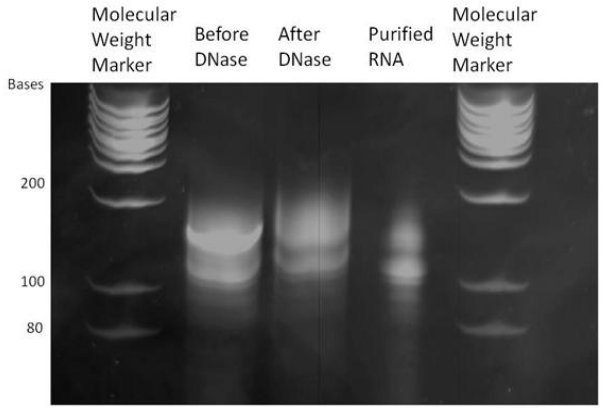


Figure 6: Denaturing Polyacrylamide Gel Indicating the Process of RNA Purification and Precipitation.
Molecular weight markers on either side of the gel were used to size the fragments. Before DNAse treatment has the highest intensity bands. After DNAse treatment, the bands are fainter. Purified RNA is the precipitated RNA after G50 purification.

3.3. Computational Analysis of Aptamer Secondary Structure

The secondary structure of the aptamers was predicted using MFOLD. MFOLD predicts the minimum free energy, ΔG, required for conformational stability at 37 °C (Zuker 2003). For

each aptamer, between one and five conformations were predicted. P2 had five predicted stable structures, P10 had four, B65 and B11 had three, T58 and B19 had two and only one was predicted for B84 (Figure 7). A structure dot plot (Appendix 1) allowed for the comparison of structural similarities and differences to be analysed. The greater the number of stable structures predicted for an aptamer, the greater the chance that some of the RNA in a solution will form arbitrary conformations and not a functional aptamer. The structure dot plots (Appendix 1) gave a value for the number of base positions that were the same in all predicted structures – this is termed the full overlap. P10 had the greatest number of overlapping nucleotides at 24, B19 followed with 22. T58 had 17 full overlaps, B11 had 12, P2 had 9 and B65 had none. Based on the number of predicted structures, B84 is the most likely as there is only one possible conformation. B65 is the least likely as there are three predicted stable conformations that share no similarity.

MFOLD generated a ΔG value for each predicted structures (Figure 7). The ΔG or the Gibbs free energy gives an indication of the structure's stability as it implies the energy available for random movement. A negative ΔG indicates a release of energy by the reaction indicating it to be more favourable. Thus the structure with the lowest (most negative) ΔG was selected as the structure with the best stability and likelihood of existence (Figure 7). B11 was the most stable with the lowest ΔG value (-26.80) (Figure 7)whilethe least stable structure predicted was for B65 (ΔG = -11.30). B84 and P2 had very similar predicted stability of ΔG = -19.05 and ΔG = -19.72, respectively. The second most stable conformation was for P10 with ΔG = -23.13. The relative order of stability based on the ΔG values was: B11, P10, P2, B84, B19, T58 and B65 (Figure 7).

The degree of structural feasibility was also determined by analysing the *pnum* values for the predicted structures. The *pmun* value for structure certainty is illustrated with base colour (Figure 7). The red and black nucleotides represent those that are most certain and the bright colours are an indication of a degree of uncertainty. The chosen structures were those with the highest certainty of conformation and those with the lowest ΔG and thus the most stable (Figure 7).

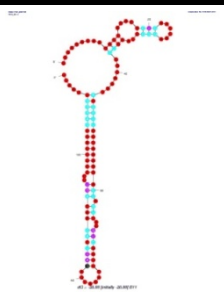
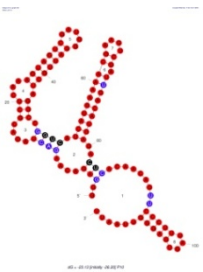
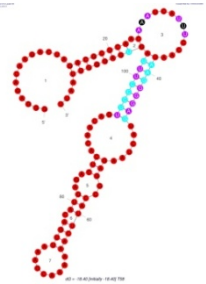
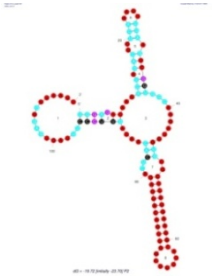
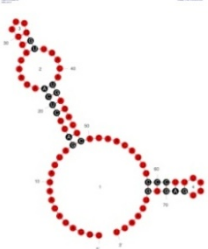
Name	Energy	Structure	Name	Energy	Structure
1. B11	ΔG = -26.80		**5. B19**	ΔG = -18.78	
2. P10	ΔG = -23.13		**6. T58**	ΔG = -18.40	
3. P2	ΔG = -19.72		**7. B65**	ΔG = -11.30	
4. B84	ΔG = -19.05				

Figure 7: Predicted Secondary Structure of Aptamers by MFOLD.
Aptamer structures as predicted by MFOLD for the most stable conformation at 37°C. Aptamers have been placed in order of their relative stability as indicated by the ΔG value. The *pnum* estimation is indicated as colours of the bases. Red and black indicate regions of conserved structure while bright colours indicate a level of uncertainty.

3.4. Expression and Purification of gp120

To determine the binding kinetics of the above mentioned aptamers, subtype C gp120 was required. Two sets of experiments were run using HIV-1_{DU151} gp120 and HIV-1_{CAP45} gp120. Only HIV-1_{DU151} gp120 was expressed for this experiment as HIV-1_{CAP45} gp120 had been previously expressed and was available for use. Glycoprotein gp120 was expressed in 293T cells and purified using affinity chromatography[1]. The purity of the HIV-1_{DU151} gp120 after affinity chromatography was determined by SDS-PAGE (Figure 8) and Western Blotting (Figure 9).

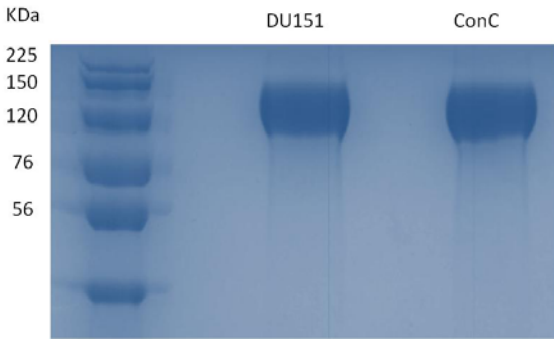


Figure 8: 8% SDS-PAGE Indicating Purified HIV-1_{DU151} gp120

SDS-PAGE stained with coomassie dye to reveal the protein bands. The molecular weight marker was used to size the proteins in the respective bands. Positive control HIV-1_{ConC} gp120 can be seen at the same height as HIV-1_{DU151} gp120.

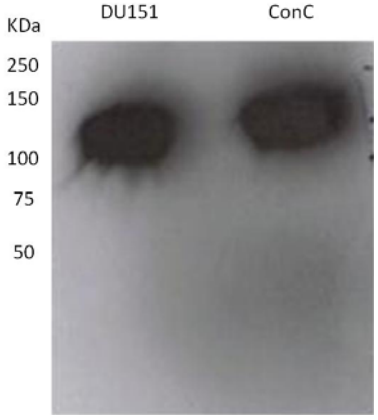


Figure 9: Western Blot of HIV-1_{DU151} gp120 with Positive Control

Gp120 specific primary antibodies identified the gp120 in the western blot. HIV-1_{ConC} gp120, was used as the possitive control. HIV-1_{DU151} gp120 and HIV-1_{ConC} gp120 were detected by the immunoflourescent assay.

SDS-PAGE was used to verify that the protein produced was of the correct size (Figure 8). HIV-1_{ConC} gp120 was used as a positive control in both experiments as it is a HIV-1 subtype C protein of the same size. HIV-1_{DU151} gp120 had the same apparent molecular weight as HIV-1_{ConC} gp120 as shown in Figure 8. The Western blot was probed with pooled serum from HIV positive individuals (HIV IgG) because it contained antibodies specific to gp120. The HIV-1_{DU151} gp120 band corresponding to the positive control, HIV-1_{ConC} gp120, on the Western blot confirmed the presence HIV-1_{DU151} gp120 (Figure 9). This protein was used for gp120 binding kinetics.

[1] Due to time constraints the purification by affinity chromatography was performed by other individuals from the laboratory.

3.5. Validation of gp120 by Binding to IgG b12

To validate the biological activity of gp120, the protein was tested for binding to b12 monoclonal antibody (Figure 10). The monoclonal antibody (IgG b12) recognises an epitope that overlaps the CD4 binding site and competes with the primary HIV-1 receptor for binding (Burton 1994). IgG b12 is a conformation specific antibody that contains cross-clade neutralising activity against different HIV-1 subtypes (Trkola 1995). The BIAcore sensorgram reached a maximum at which point the graph reached a plateau relative to the concentration of the antibody injected. When the injection was stopped, the RU decreased as there was no longer analyte passing through the flow cell diffracting the laser (Figure 10). The difference between before injection and after injection is the ΔRU and indicates the level of binding. In this case, IgG b12 bound with 935 RU (Figure 10). Binding of IgG b12 to gp120 indicated that the protein was correctly folded and could be used for subsequent experiments.

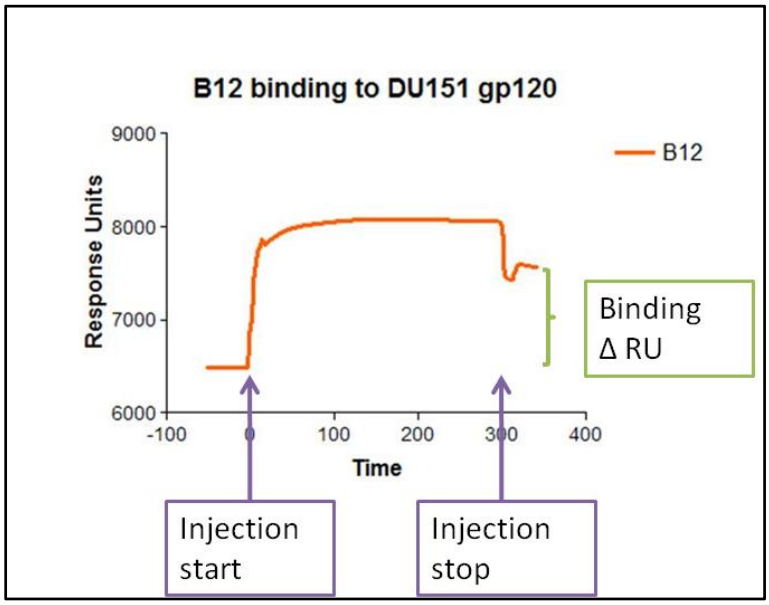


Figure 10: Monoclonal b12 Antibody Binding HIV-1_{DU151} gp120.
The y axis is in response units and the x axis is time in seconds. The start and stop injection point are indicated on the graph. An increase in RU is seen after injection and a decrease is seen after the injection has stopped. The plateau after injection corresponds to the concentration of injected analyte. The graph was corrected for non-specific binding by removing the control flow cell. B12 bound with high affinity and 935 RU.

3.6. Aptamers Isolated against HIV-1_{BA-L} gp120 Bound Monomeric HIV-1_{DU151} gp120

The aptamers raised against HIV-1_{BA-L} were tested for binding to HIV-1_{DU151} gp120. Binding to HIV-1_{DU151} gp120 had to be confirmed before a kinetic analysis could follow. SPR was used to determine aptamer-gp120 kinetics. Of the four flow cells available, three had HIV-1_{DU151} gp120 immobilised and the fourth had no protein. The no-protein control was included

to correct for non-specific binding to the chip surface. The control graph was included to highlight the binding of the aptamer to the protein. Each aptamer was shown to bind with differing affinity and those that did not bind were excluded from further analysis (Figure 11).

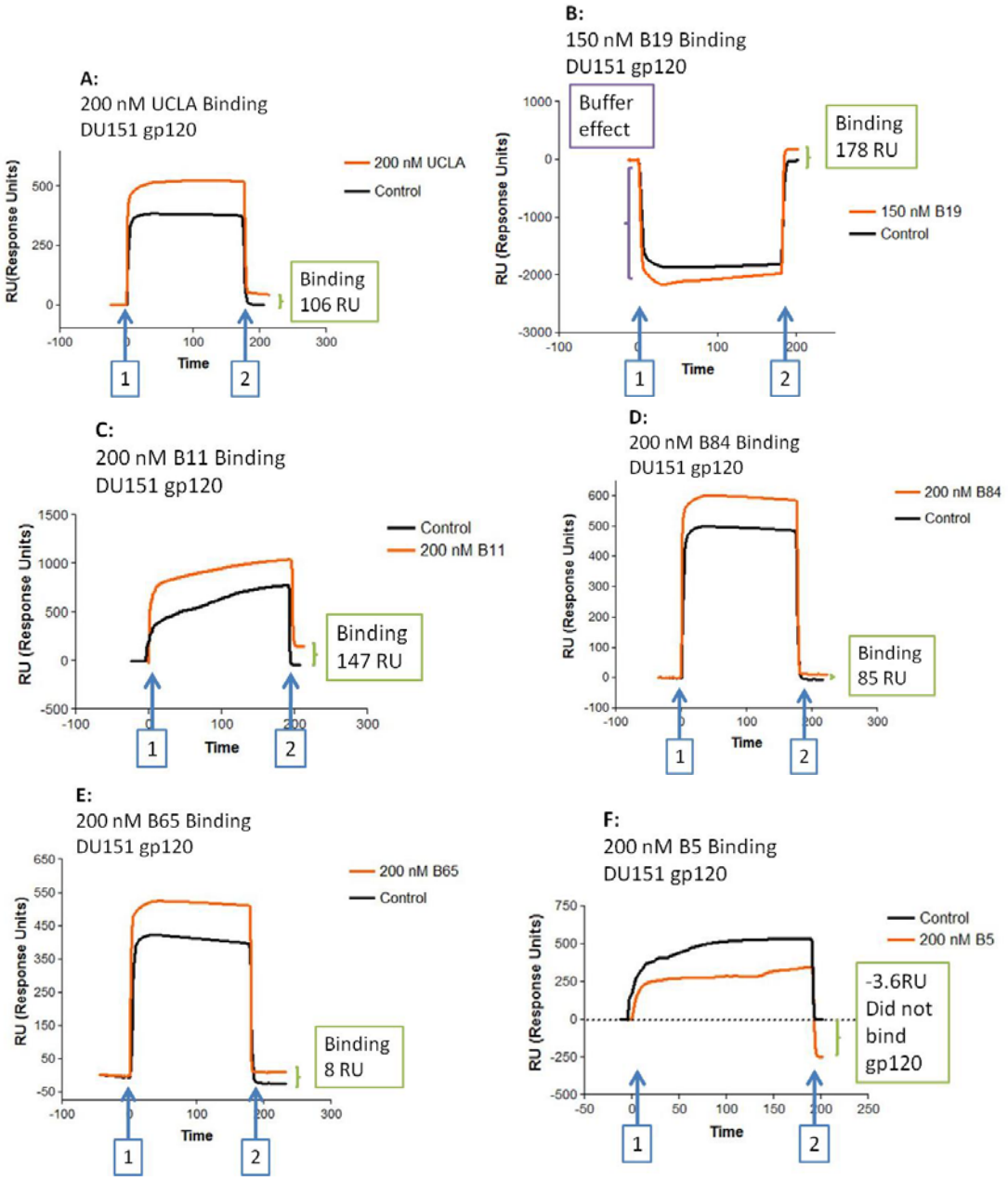


Figure 11: Aptamers Raised Against HIV-1_{BA-L} Binding to HIV-1_{DU151} gp120

The y axis is response units and the x axis time in seconds. Sensorgrams edited in BIAevaluation indicating the level of binding of each aptamer to immobilised HIV-1_{DU151} gp120. Injection start and stop points are indicated by 1 and 2 respectively. Binding curves increase after injection (A, C, D, E and F) indicating a change in the refractive index of the laser due to the analyte passing the sensor. The drop after injection indicates that the analyte is no longer passing the sensor. Sensorgrams drop according to the amount of aptamer bound to the chip surface. The experimental curves are higher than the control where the aptamer bound. The control curve returned to base line after injection has finished as no aptamer has bound. A: 200 nM UCLA bound with 106 RU B: 150 nM B19 bound with 178 RU. There was a drop in RU after injection which was attributed to the buffer effect. C: 200 nM B11 bound with 147 RU. D: 200 nM B84 bound with 85 RU. E: 200 nM B65 bound with 8 RU. F: 200 nM B5 did not bind DU151 gp120. The experimental curve drops below the starting line indicting that immobilised protein may have dislodged during injection.

The injection start and stop points are indicated as 1 and 2 respectively (Figure 11). The binding experiments were conducted using 200 nM of each aptamer injected for 3 minutes. For the binding test of B19, 150 nM was used as there was difficulty in transcribing this aptamer and so it was conserved for the kinetics experiment for which a large amount of RNA was required. The concentration was decided on because it has been previously shown to be sufficient for stable binding. There was an increase in the RU at the point of injection due to the analyte passing over the sensor surface which caused a change in the refractive index of the laser (Figure 11: A, C, D, E and F). This was true for both the control and experimental flow cells. In Figure 11: B after injection a drop in response units was seen. The drop is caused by the buffer shifting the refraction index in the opposite direction and is termed the buffer effect. After the drop, association was seen as B19 was binding to the protein. After the injection stopped, the RU increased vertically to the level of binding (Figure 11: B).

The RU level seen on the graph after injection indicated the level of aptamer binding to the protein. The difference between control and experimental flow cells was the level of binding, expressed as RU (Figure 11). Aptamers B19, B65, B84, B11 and UCLA were shown to bind HIV-1_{DU151} gp120 with varying RUs (Figure 11: A – E). B5 did not bind and the experimental sensorgram ended below that of the control (Figure 11: F). This may indicate that the immobilised protein was dislodged during the experiment.

The control sensorgram is expected to start and end at the same RU level as no binding is expected however, this is not always the case due to non-specific associations. As B5 did not bind HIV-1_{DU151} gp120 (-3.6 RU) it was excluded from further analysis. The remaining aptamers bound to gp120 with the following RU: 106 RU UCLA, 147 RU B11, 178 RU B19, 85 RU B84, and 8 RU B65. These aptamers were used for kinetic analysis on DU151 gp120.

3.7. Aptamers Isolated against Whole HIV-1_{CAP45} gp120 Bound HIV-1_{CAP45} Monomeric gp120

P2, P10 and T58 were raised against a whole pseudovirus expressing Env from R5 virus called HIV-1_{CAP45}. These aptamers were tested for binding to monomeric gp120 immobilised to a CM5 chip using BIAcore SPR (Figure 12). Binding was analysed with 200 nM concentrations of each aptamer injected over the protein for 3 minutes. Although the

aptamers were raised against the whole HIV-1_{CAP45} glycoprotein, it is possible that they would not bind the HIV-1_{CAP45} gp120 monomer.

The injection start and stop sites are indicated by 1 and 2 respectively (Figure 12). After injection there was an increase in the RU for all binding graphs (Figure 12: A, B and C). The RUs reached a plateau shortly after injecting P10 (Figure 12: A) indicating a saturation of the chip. For P2 and T58 (Figure 12: B and C) no plateau was reached indicating that the aptamers had the capacity to bind more. T58 showed the best binding with 739 RU followed by P2 with 351 RU and lastly P10 with 90 RU (Figure 12). All three aptamers were used in the kinetic analysis on HIV-1_{CAP45} gp120.

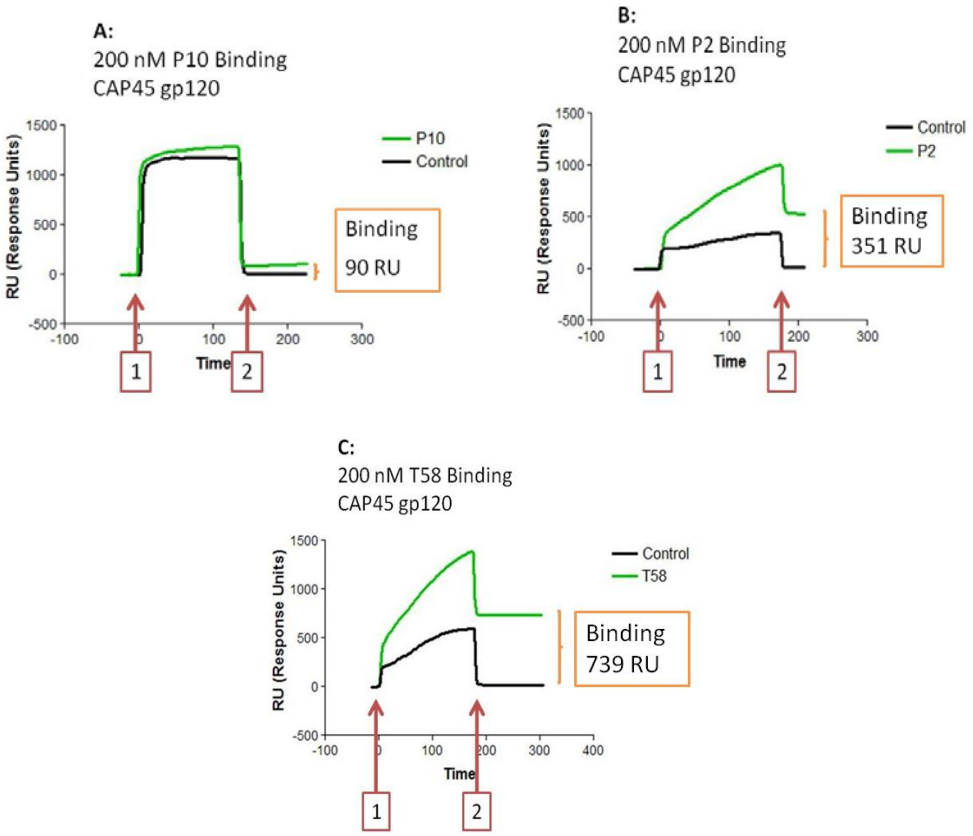


Figure 12: Aptamer Binding to HIV-1_{CAP45} gp120
The y axis is response units and the x axis time in seconds. Aptamer injection start and stop points are indicated by 1 and 2 respectively. A: 200 nM P10 binding with 90 RU. A plateau is reached that corresponds to aptamer concentration. B: 200 nM P2 binding with 351 RU. No plateau is reached as aptamer has capacity to bind more. C: 200 nM T58 binding with 739 RU. No plateau is reached as aptamer has capacity to bind more.

3.8. Optimisation of Kinetics Using UCLA on HIV-1_{DU151} gp120

The binding kinetics of aptamers shown to bind monomeric gp120 was determined using BIAcore SPR technology. The level of protein immobilisation and the flow rate were optimised using UCLA against monomeric HIV-1_{DU151} gp120. UCLA was used as a positive

control aptamer as it is known to bind with high efficiency to gp120. If there is high surface density of ligand on the chip and the flow rate is too slow, the rate of anylate binding may exceed the rate at which it is delivered. This is termed mass transport limitation and can negatively affect the kinetic readings and yield a slowed apparent k_{on} than is true.

To determine the correct level of protein immobilisation needed for kinetic analysis, three flow cells with different levels of protein immobilised were used. Initially, the lowest possible response units were used (300 RU, 800 RU and 1500 RU immobilised protein). However, for the purpose of this study, no data was obtained when the response units were set that low as seen in Figure 13. The injection start and stop point are indicated by 1 and 2 respectively (Figure 13). An increase in RU was seen for each concentration of UCLA after injection which decreased back to the base line after injection had stopped, indicating that no aptamer was bound to the protein (Figure 13). After the injection of 10 nM UCLA the RU spiked higher than that of the other concentrations of UCLA (Figure 13). It was concluded that as gp120 is a relatively large molecule it may cause a large change in RU with minimal binding and so there was insufficient protein immobilised on the chip for aptamer binding. The spike seen with the injection of 10 nM aptamer was regarded as a reading anomaly and the experiment was repeated with altered conditions to correct for this. Protein immobilisation was increased to 3000 RU, 13 000 RU and 23 000 RU for the second optimisation experiment.

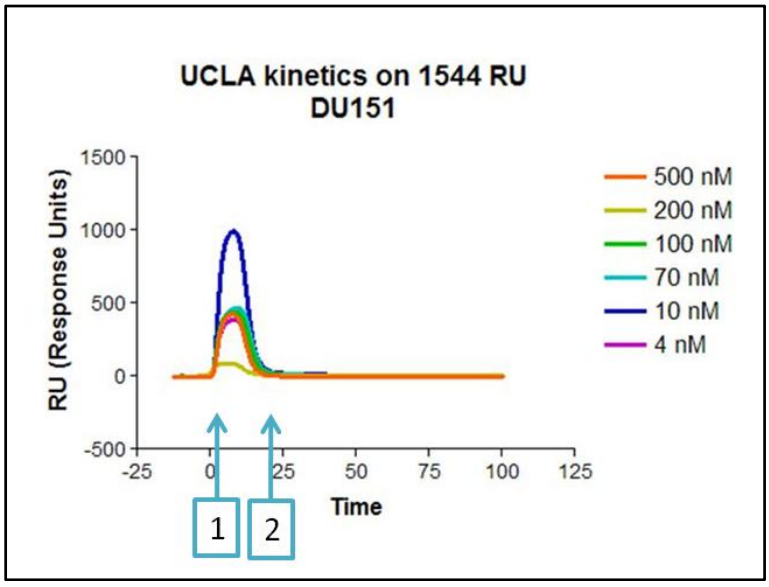


Figure 13: UCLA Binding Kinetics on Minimum Protein Response Units.
The y axis represents response units and the x axis is time in seconds. The injection start and stop points are indicated by 1 and 2 respectively. The coloured lines indicate the different UCLA concentrations injected over the protein. Each aptamer concentration is seen to increase after injection and decrease back to base line after injection has stopped. There was no change in RU before and after injection indicating no binding to the chip.

The chip was activated with EDC:NHS which allowed for the protein to be bound by amine coupling. Once activated, the protein was injected onto three flow cells at different immobilisation levels. The remaining activated sites on the chip were blocked by ethanolamine before Glycine-HCl was injected to remove any partially bound protein. Each stage of preparation caused a shift in the refractive index (Figure 14). The resultant RU related to the level of immobilised protein. The control flow cell remained at baseline as no protein was injected.

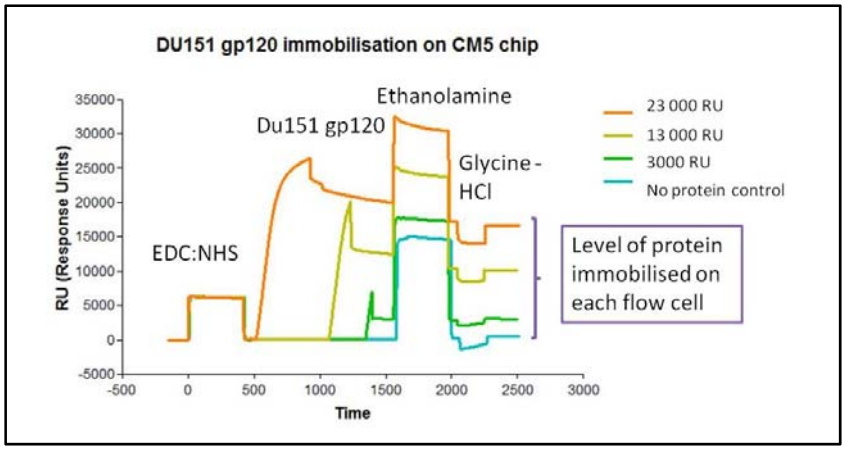


Figure 14: Preparation of CM5 Chip for Kinetic Analysis of UCLA on HIV-1_{DU151} gp120.
The y axis is response units and the x axis time in seconds. EDC:NHS activated the chip prior to protein binding. A different amount of protein was injected into three flow cells with a fourth with no protein. Ethanolamine blocked any remaining active sites and Glycine-HCl knocked off weakly bound protein. The resultant RU indicates the amount of protein immobilised on each flow cell. The flow cells had 23 000 RU, 13 00 RU and 3 000 RU immobilised.

The different aptamer concentrations were injected in ascending order over all four flow cells. The standard deviation for each experimental condition could not be calculated as no repetitions were included. The dissociation constant (K_d) was obtained for each flow cell independently. The K_d was calculated (by BIAevaluation software) using the k(on), k(off) values and aptamer concentrations. The k(off) represents the global dissociation value calculated for the dissociation of the aptamer in each flow cell. This value was calculated independent of aptamer concentration and association. The k(on) value takes into account the k(off) and the aptamer concentrations used and was a global association value. The Chi^2 value associated with each calculation gave an indication of goodness of fit with a value of 1. The k(on) and k(off) were calculated separately using the 1:1 Langmuir Binding Model and a Chi^2 value was calculated for each step. The same method of kinetic analysis was applied when analysing the results of all kinetics experiments.

The result for flow cells immobilised with 23 000 RU and 13 000 RU was very similar and the associated Chi^2 values indicated confidence in the result (Table 4). The aptamers separated in a concentration dependent manner with the highest injected concentrations having the highest RU (Figure 15).

Table 4: Calculated Constants and Associated Chi^2 Values for UCLA Kinetics on HIV-1_{DU151} gp120

K(off) – calculated value for ligand dissociation, not dependent on Concentration and k(on)
K(on) – calculated value for ligand association based on Concentration and k(off)
K_d – dissociation constant for the reaction calculated using the Concentration, k(on) and k(off)

Protein RU	Flow Cell	k(off)	Chi^2	k(on)	Chi^2	K_d
23 000	1	0.015	1.9	4.42e5	0.2	3.39e-8
13 000	2	0.015	0.347	4.26e5	0.04	3.52e-8
3000	3	0.015	0.289	6.53e5	4.22e3	2.3e-8

The association appeared rapid with a steep incline while the dissociation was slower with a duller gradient. After 150 seconds the dissociation became gradual and the aptamer remained stably bound to the protein for both flow cell immobilisations (Figure 15). The K_d calculated for the flow cell with 23 000 RU gp120 was 33.9 nM (Figure 15: A) and for 13 000 RU gp120 was 35.2 nM (Figure 15: B).

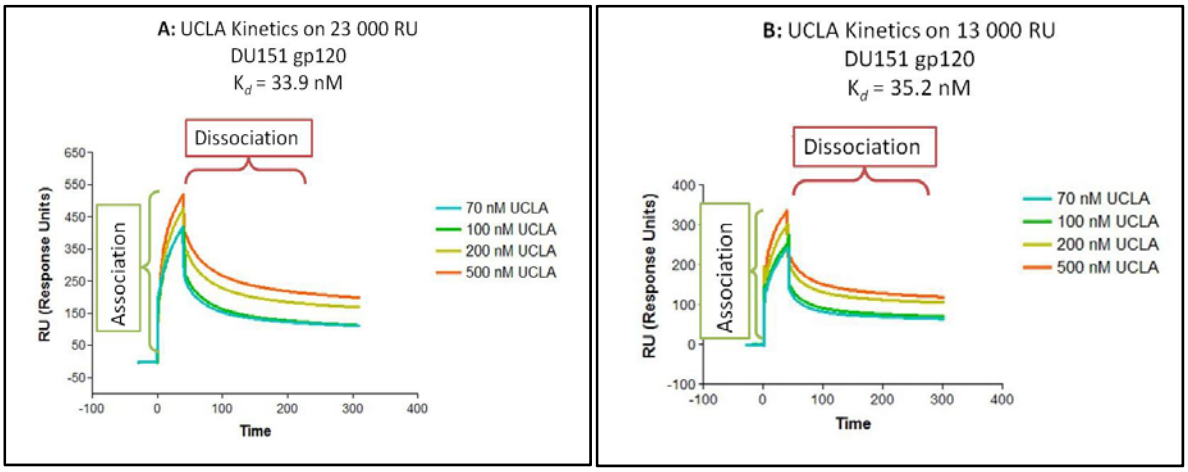


Figure 15: UCLA Binding Kinetics on HIV-1_{DU151} gp120.
The y axis indicated the response units caused by binding to the protein. The x axis shows time in seconds. The coloured lines indicate the different aptamer Concentrations injected over the immobilised protein. The association and dissociation periods have been highlighted on each graph. A: UCLA kinetics on 23 000 RU HIV-1_{DU151} gp120. The resultant K_d was calculated as 33.9 nM. B: UCLA kinetics on 13 000 RU DU151 gp120. The resultant K_d was calculated as 35.2 nM.

When kinetics data was obtained from the flow cell with 3000 RU gp120, the K_d decreased to 23 nM (Figure 16). More notably, the graph for 3000 RU immobilised inverted

where higher concentration aptamers appeared to bind less than the lower concentration aptamers resulting in lower RU after dissociation (Figure 16). The dissociation appeared much more rapid than on the flow cells with more protein immobilised (Figure 16). The Chi^2 value for the calculated k(on) was 3 orders of magnitude larger than that of the other two experimental flow cells indicating reduced confidence in the accuracy of the result (Table 4). It was concluded that 3000 RU of immobilised protein was below the minimum requirement for adequate binding and thus for further kinetics studies 13 000 RU – 23 000 RU immobilised gp120 was used.

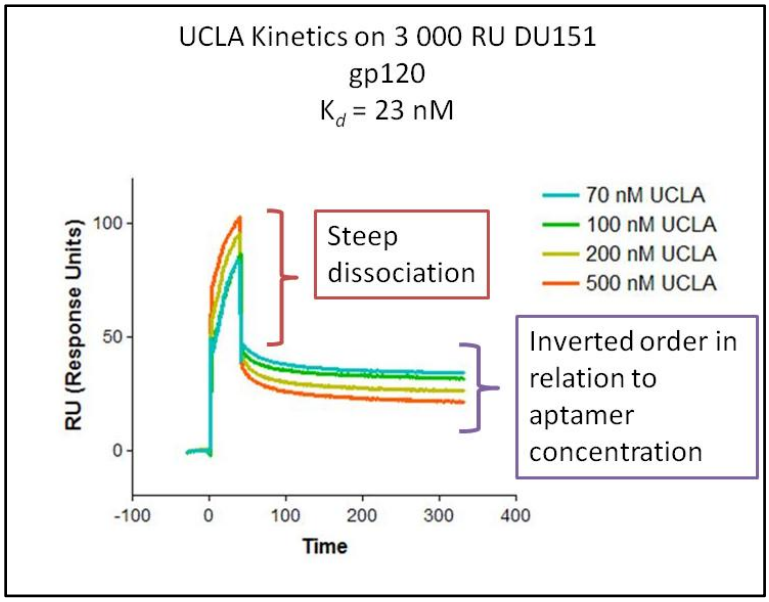


Figure 16: UCLA Binding Kinetics on 3000 RU HIV-1_{DU151} gp120
The y axis is in response units and the x axis is time in seconds. The dissociation gradient was very steep indicated in red on the graph. The coloured lines indicate the different UCLA concentrations injected over the protein. The curves separated according to concentration but the lowest concentration aptamer resulted in the highest RU. The resultant K_d was calculated as 23 nM.

3.9. Further Optimisation of Kinetics on HIV-1_{DU151} gp120

The parameters determined for UCLA on HIV-1_{DU151} gp120 provided the foundation for further optimisation. The concentration of aptamer injected over the immobilised protein was optimised using B84, B65 and B19 on HIV-1_{DU151} gp120. Optimisation was conducted in triplicate so a statistical analysis could be applied to the results and the standard deviation calculated. The chip was activated with EDC:NHS prior to binding protein to three flow cells, a fourth contained no protein (Figure 17). The same amount of protein was immobilised to three flow cells. The remaining active sites were blocked with ethanolamine and the weakly bound protein was removed with a Glycine-HCl wash (Figure 17).

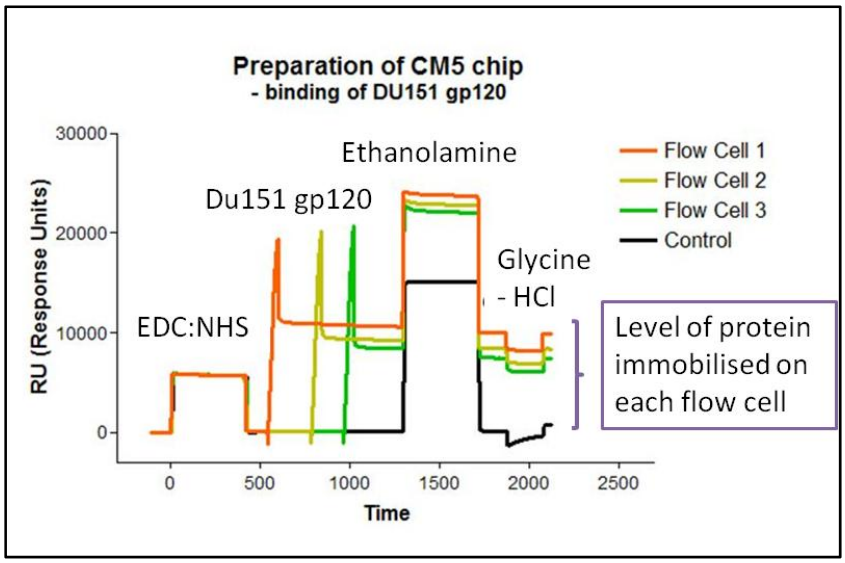


Figure 17: Preparation of CM5 Chip for Kinetics Experiments
The y axis is response units and the x axis time in seconds. The chip was activated with EDC:NHS before protein was injected into three flow cells. The same amount of protein was injected into three flow cells and a fourth had no protein. Ethanolamine blocked remaining active sites and Glycine-HCl removed weakly bound protein. The protein RU for the three flow cells differed slightly.

Initial experiments used B65, B19 and B84 and identified that 13 000 RU immobilised protein was insufficient for kinetic analysis (outlined in Appendix 2). They also showed that although 500 nM UCLA bound with high affinity to the immobilised protein, this was too high for the aptamers used in this study (Appendix 2). These kinetic experiments generated very low K_d values with very high associated Chi^2 values. The associated kinetics graphs showed a discrepancy in the expected profile when the aptamer concentrations used for the UCLA optimisation experiment were used (Appendix 2).

Further optimisation of aptamer concentration used only B84 as it transcribed with the highest efficiency. Briefly, three concurrent flow cells were loaded with 13 000 RU HIV-1_{DU151} gp120. The aptamer kinetics was determined to fit the 1:1 Langmuir binding model; however the associated graph illustrated the incorrect binding profile (Appendix 2). While the more concentrated aptamer solutions are expected to end with the highest RU, the graph demonstrated a different but not fully inverted profile (Appendix 2: Figure iii). The 200 nM and 500 nM solutions grouped together below 70 nM and above 30 nM. It was concluded that these concentrations were too high for aptamer binding due to increased competition for binding. An excess of aptamer injected over the protein surface may result in unbound aptamer knocking off the bound aptamer as it passes the chip surface. To test this, a reduction in aptamer concentration was explored to correct this.

A 70 nM concentration was chosen as the upper limit decreasing with half log dilutions to 0.5 nM (Appendix 2: Figure iv). Below 14 nM the aptamer was unable to cause a significant change in the refractive index and a result was not given which lead to the inversion of the expected binding profile (Appendix 2: Figure iv). A further kinetic experiment was set up with the upper concentration limit of 70 nM and the lower concentration limit of 14 nM (Appendix 2: Figure v). This proved to be too narrow a window for meaningful results as selected concentrations were too similar to produce a valid K_d (calculated as 2.84×10^3 nM ± 2.1×10^3). It was thus decided to raise the upper concentration limit to 150 nM chosen based on previous experiments showing partial success of 100 nM and 200 nM. To generate a minimum of five data points a 2 fold dilution was used resulting in concentrations of 150 nM, 75 nM, 37 nM, 18.5 nM, 9 nM, 4.5 nM. This experiment proved successful (results outlined in 3.10.1.) and the parameters were then used in all subsequent kinetics experiments.

3.10. Aptamer Binding Kinetics on HIV-1_{DU151} gp120

B11, B65 and B84 binding kineticswere determined on HIV-1_{DU151} gp120. Insufficient B19 was generated for kinetic analysis and so was excluded even though it bound monomeric HIV-1_{DU151} gp120. The parameters determined in the optimisation experiments outlined in 3.8 and 3.9 were used for kinetic experiments on both HIV-1_{CAP45} gp120 and HIV-1_{DU151} gp120. BIAevaluation software was used to analyse the results and the empty flow cell was deducted from the experimental results to correct for non-specific binding and instrument noise. The separate ka / kd kinetic analysis tool was used to calculate the K_d and associated Chi^2 values. The 1:1 Langmuir Binding model was used for the calculation of the K_d. This model states that for each ligand there can only be one analyte bound. The results were expressed as sensorgrams indicating the association and dissociation period of the aptamer concentrations to the protein.

3.10.1. B84 Kinetics on HIV-1_{DU151} gp120

B84 bound to monomeric HIV-1_{DU151} gp120 with the second lowest RU of 85 RU. The association of B84 followed a concentration dependent gradient for most injected concentrations (Figure 18). The final binding RU for the aptamer concentrations distributed according to concentration except for 150 nM and 9 nM (Figure 18). At 150 nM the dissociation ended below the lower aptamer concentrations. This concentration may be too high for B84 binding. The 9 nM injection did not follow the same gradient as the other

concentrations (Figure 18). The association of 9 nM peaked higher than expected and the binding appeared stronger than expected (Figure 18). This result may have been due to some of the anylate from the previous flow through remaining bound to the chip surface compounding the binding response. This was not seen with the following injection (Figure 18, 18.5 nM) indicating that the bound aptamer was fully removed prior to subsequent injections. The other aptamer concentrations follow a concentration dependent binding pattern (Figure 18). . The dissociation of each of the concentrations was steady and the aptamer remained bound after 50 seconds (Figure 18) indicating a stable interaction. The K_d for B84 binding was calculated to be 23 nM ± 8 with the associated Chi^2 values within the range of statistical significance (Table 5).

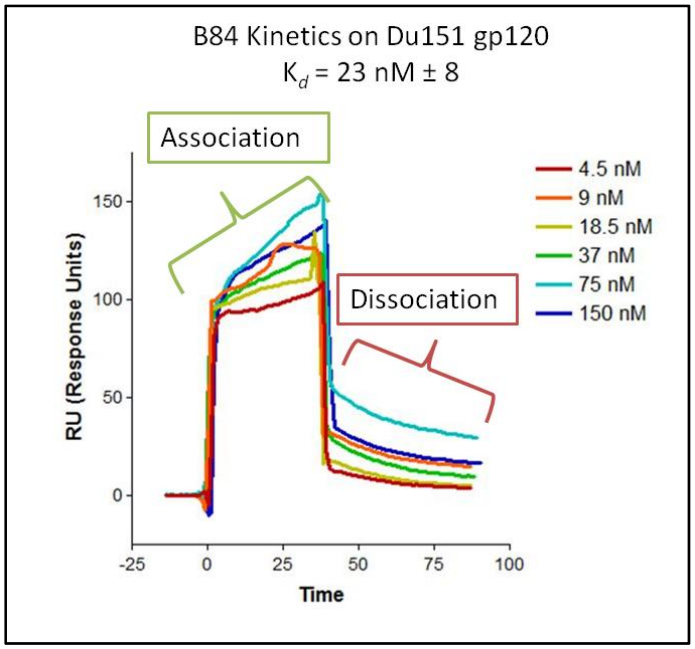


Figure 18: B84 Binding Kinetics on HIV-1_{DU151} gp120 with Increased Concentration Limits.

The y axis is response units and the x axis time in seconds. Association and dissociation regions are indicated. Each coloured line represents a different concentration of B84 injected. All aptamer concentrations dissociate slowly after injection has stopped. The different aptamer concentrations are clearly distinguished from one another. The higher concentration aptamers result in higher RU.

Table 5: Calculated Constants and Associated Chi^2 Values for B84 Kinetics on HIV-1_{DU151} gp120.

Flow Cell	k(off)	Chi^2	k(on)	Chi^2	K_d
1	0.0209	0.296	1.06e-6	0.947	1.97e-8
2	0.0248	0.124	1.43e-6	0.244	1.73e-8
3	0.0211	0.744	5.91e-6	1.34	3.57e-8
AVERAGE	0.0222	0.388	2.8e-6	0.843	2.3e-8

3.10.2. *B65 Kinetics on HIV-1_{DU151} gp120*

B65 showed very low binding to HIV-1_{DU151} gp120 of 8 RU but was included for kinetic analysis to determine the effect of low RU on kinetic analysis. Although from the statistical analysis the resultant K_d was statistically significant (Table 6), the curve provided little confidence in the result (Figure 19). The association of each aptamer concentration was erratic and the curve showed many peaks and deviations (Figure 19). The RU change was not a reflection of the concentration injected and 4 nM resulted in a higher association RU than all greater concentrations with the exception of 300 nM (Figure 19). The dissociation phase again did not represent the concentration dependent RU result as the high and low concentrations grouped together in an erratic manner (Figure 19). This may indicate that a low RU binder is not a good candidate for kinetic analysis even if a statistically relevant result can be obtained. The statistical values associated to the calculated k(on) and k(off), used for the K_d calculation were not supported by the sensorgram (Table 6).

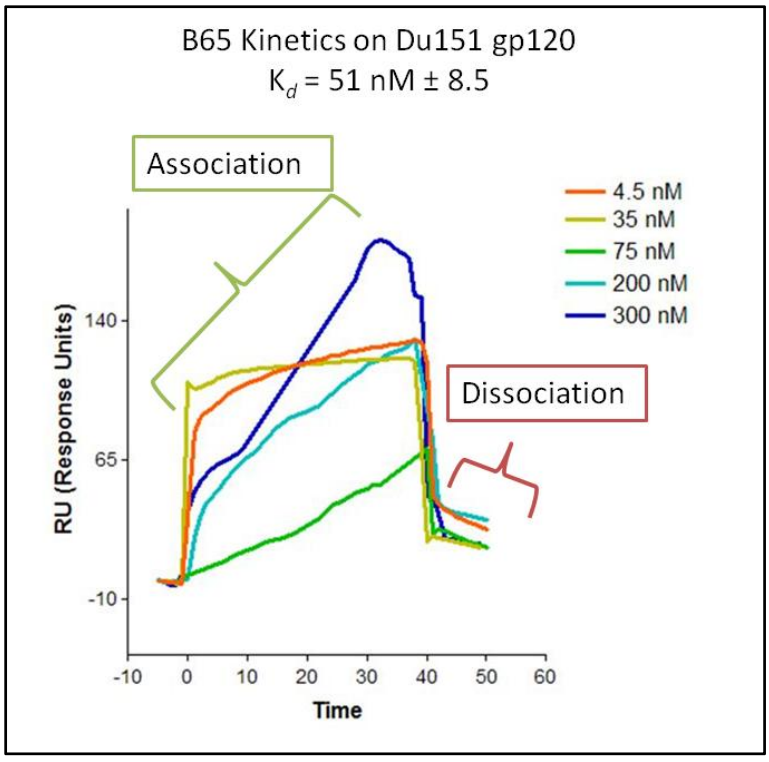


Figure 19: B65 Binding Kinetics on HIV-1_{DU151} gp120.
The y axis is response units and the x axis is time in seconds. The coloured lines indicate the different P10 concentrations injected over the protein. The RU change was not a reflection of the concentration injected. The association and dissociation periods are indicated. The association period is erratic and each aptamer concentration had a different gradient. The dissociation is not according to injected concentration. All aptamer concentrations end above the baseline. There is a steep gradient during the dissociation phase.

Table 6: Calculated Constants and Associated Chi^2 Values for B65 Kinetics on HIV-1$_{DU151}$ gp120.

Flow Cell	k(off)	Chi^2	k(on)	Chi^2	K_d
1	9.61e-3	1.36	1.77e5	0	5.43e-8
2	8.41e-3	0.983	2.07e5	0	4.06e-8
3	8.43e-3	1.23	1.43e5	0	5.88e-8
AVERAGE	8.82e-3	1.19	1.76e5	0	5.12e-8

3.10.3. *B11 Kinetics on HIV-1$_{DU151}$ gp120*

B11 was shown to bind to HIV-1$_{DU151}$ gp120 with 147 RU and was the second highest value for binding to HIV-1$_{DU151}$ gp120. The kinetic analysis of B11 revealed it as a weaker binder than the other aptamers tested on HIV-1$_{DU151}$ gp120 (K_d = 179 nM ± 81) (Figure 20).

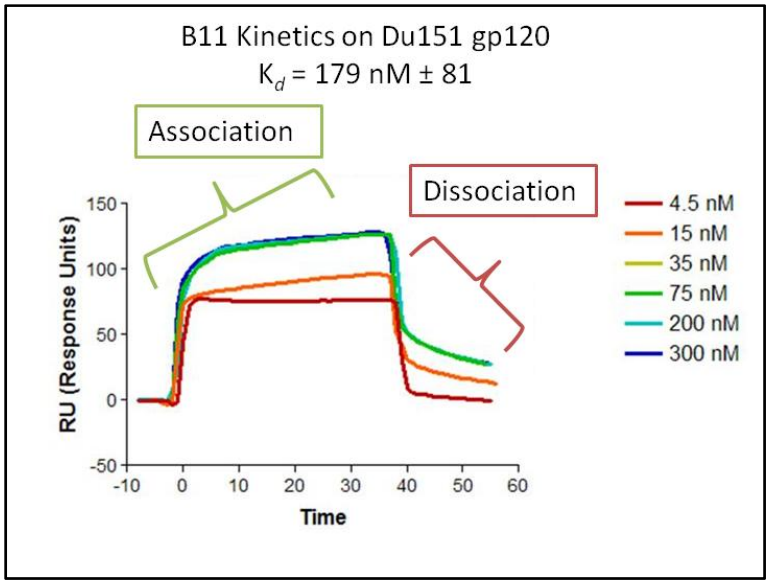


Figure 20: B11 Binding Kinetics on HIV-1$_{DU151}$ gp120.
The y axis is response units and the x axis time in seconds. The association and dissociation periods are indicated. Each coloured graph indicates a different B11 concentration injected. All concentrations had a steep dissociation and a mild association gradient. Higher concentration aptamers grouped at the same RU while differentiation was seen between the lower concentrations. The K_d was calculated as 179 nM ± 81.

The association and dissociation periods are indicated on the graph (Figure 20). The dissociation of all aptamer concentrations was rapid with the lowest concentration (4.5 nM) falling down to the base line (Figure 20). This rapid dissociation, indicative of weak interaction strength was confirmed by the calculated K_d. The higher concentration aptamers (75 nM, 200 nM and 300 nM) group together during both the association and dissociation phases (Figure 20).

Table 7: Calculated Constants and Associated Chi^2 Values for B11 Kinetics on HIV-1$_{DU151}$ gp120.

Flow Cell	k(off)	Chi^2	k(on)	Chi^2	K_d
1	0.0376	0.988	1.89e5	0	1.99e-7
2	0.0345	1.41	1.33e5	0	2.59e-7
3	0.0392	1.25	6.95e5	0	7.95e-8
AVERAGE	0.0371	1.216	3.39e5	0	1.79e-7

The association of each concentration was very gradual which may indicate a low affinity for the protein indicated by the calculated k(on) value (average 3.39e5) (Table 7). Of all aptamers tested on HIV-1$_{DU151}$ gp120, B11 showed the highest K_d even though the binding RU was among the highest.

3.11. Aptamer Kinetics on HIV-1$_{CAP45}$ gp120

The aptamers raised against HIV-1$_{CAP45}$ pseudovirus (P10, T58, P2) were tested for binding to monomeric HIV-1$_{CAP45}$ gp120. All three aptamers were found to bind with varying RU (90 RU to 739 RU). The parameters identified in the optimisation experiments on HIV-1$_{DU151}$ gp120 were used for the kinetic analysis on HIV-1$_{CAP45}$ gp120. For each aptamer, concentrations ranging from 5 nM to 300 nM were injected over four flow cells on a research grade CM5 chip. Three flow cells loaded with 20 000 RU immobilised protein and the fourth flow cell contained no protein. The no protein control was used to correct for non-specific binding to the chip and instrumental noise. The results were expressed as sensorgrams indicating the association and dissociation period of the aptamer concentrations to the protein. All aptamers were analysed using the separate ka/ kd analysis tool using the 1:1 Langmuir Binding Model.

3.11.1. P10 Kinetics on HIV-1$_{CAP45}$ gp120

P10, the weakest binder of the three HIV-1$_{CAP45}$ aptamers revealed the highest K_d of 221 nM ± 81. The aptamer started to dissociate before the full association time had passed (Figure 21). This is a clear indication of its loose binding to the protein. The higher concentrations (100 nM and 200 nM) did not form distinct lines and ended at the same RU after dissociation (Figure 21). The lower concentrations (5 nM to 50 nM) also ended at the same point but much closer to the base line (Figure 21). The lower concentration aptamers appeared to have

almost fully dissociated from the protein 50 seconds after injection stopped while the higher concentration aptamers remained bound with 50 RU (Figure 21). The associated statistical analysis indicated confidence in the result (Table 8). The Chi^2 associated with the k(on) for all flow cells was 0 and for k(off) was close to 1.

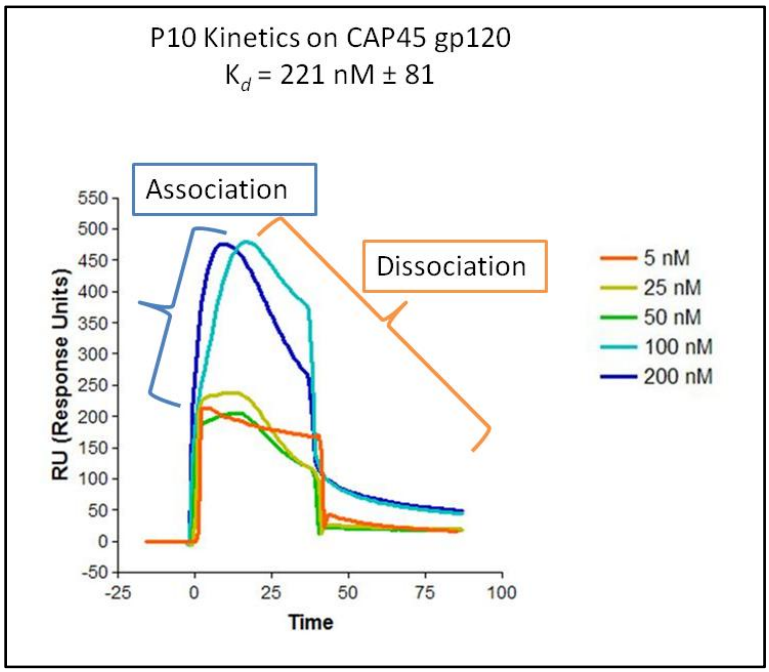


Figure 21: P10 Binding Kinetics on HIV-1_{CAP45} gp120.
The y axis is response units and the x axis time in seconds. The association and dissociation periods are indicated on the graph. The coloured lines indicate the different P10 concentrations injected over the protein. Dissociation of all aptamer concentrations appears to start before injection is finished. The lower concentration aptamers appear to have almost fully dissociated 50 seconds after injection is stopped. The higher concentration aptamers remain bound although with low RU. The resultant K_d was 221 nM ± 81.

Table 8: Calculated Constants and Associated Chi^2 Values for P10 Kinetics on HIV-1_{CAP45} gp120.

Flow Cell	k(off)	Chi^2	k(on)	Chi^2	K_d
1	0.0394	1.88	1.86e5	0	2.12e-7
2	0.0438	0.892	1.39e5	0	3.16e-7
3	0.0397	1.78	2.95e5	0	1.35e-7
AVERAGE	0.041	1.52	2.07e5	0	2.21e-7

3.11.2. T58 Kinetics on HIV-1_{CAP45} gp120

T58 bound with the highest RU of all aptamers tested against HIV-1_{CAP45} gp120 with 739 RU. Kinetics curves indicated that T58 did not dissociate rapidly from HIV-1_{CAP45} gp120 (Figure 22). The dissociation phase had a very slight gradient indicating a slow dissociation

from the protein. The aptamers separated in a concentration dependent manner with clear distinction between the upper concentrations however, the lower concentrations (18 nM and 37.5 nM) cannot easily be individually distinguished (Figure 22).

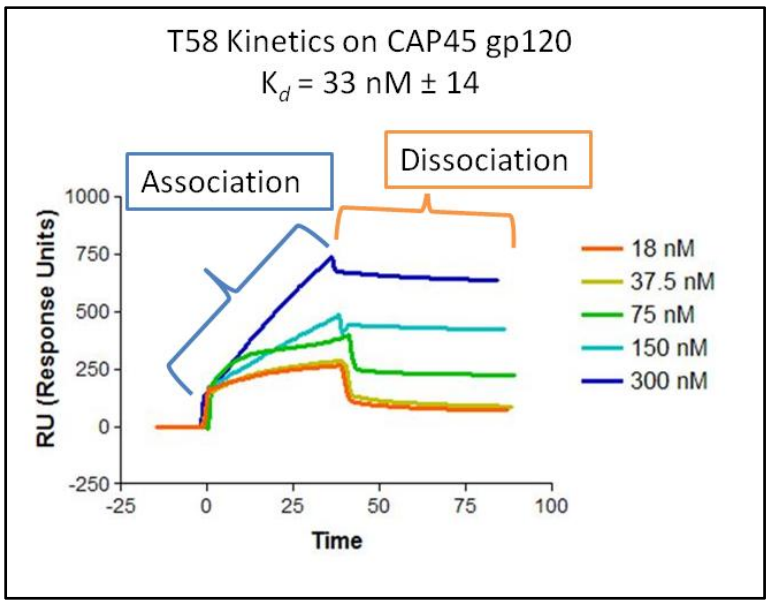


Figure 22: T58 Binding Kinetics on HIV-1_{CAP45} gp120.
The y axis is response units and the x axis time in seconds. The coloured lines indicated the different aptamer concentrations injected over the protein. The association and dissociation phases are indicated. A steep gradient is seen for the association period. All aptamer concentrations remained bound to the protein after the dissociation period.

The calculated K_d (33 nM ± 14), although relatively low, was expected to be lower as the aptamer remained stably bound after dissociation (Figure 22). The Chi^2 values associated with the k(on) and k(off) values used in the calculation of the K_d indicated confidence in the result (Table 9). The K_d calculated for T58 was similar to that of truncated B40, K_d = 31.2 nM, (Dey 2005), which is known as a strong binder of gp120.

Table 9: Calculated Constants and Associated Chi^2 Values for T58 Kinetics on HIV-1_{CAP45} gp120.

Flow Cell	k(off)	Chi^2	k(on)	Chi^2	K_d
1	3.31e-3	1.92	8.4e4	0	3.92e-8
2	2.91e-3	1.7	5.24e4	0	5.52e-8
3	3.09e-3	2.26	1.42e5	0	2.17e-8
AVERAGE	3.10e-3	1.96	9.28e4	0	3.3e-8

3.11.3. P2 Kinetics on HIV-1_{CAP45} gp120

P2 bound with 351 RU to monomeric HIV-1_{CAP45} gp120 placing it second of the three aptamers in terms of binding, after T58 and before P10. The kinetic analysis revealed P2 as the strongest binder with the tightest association (Figure 23; Table 10). The association phase had a very steep gradient in a concentration dependent manner (Figure 23).

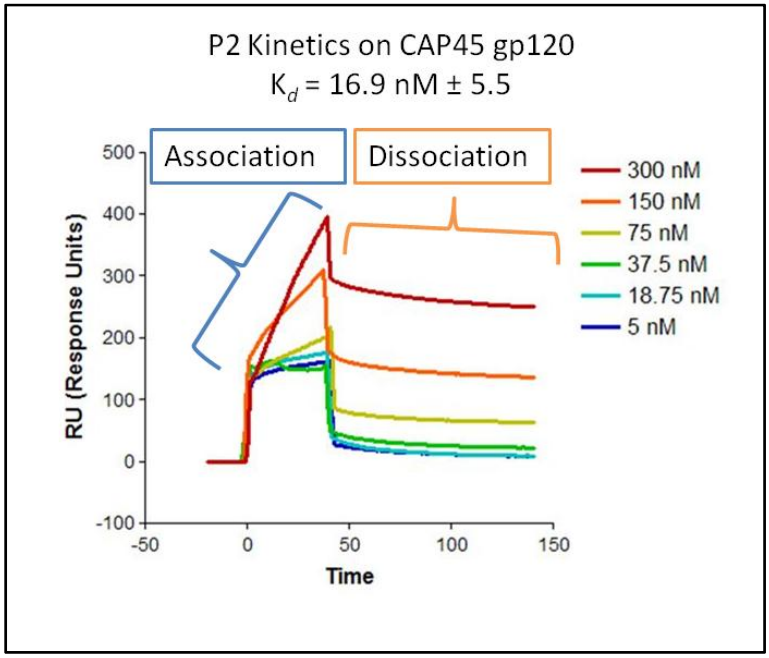


Figure 23: P2 Binding Kinetics on HIV-1_{CAP45} gp120.
The y axis is response units and the x axis time in seconds. Each coloured line indicates a different concentration of P2 injected. The association and dissociation phases are indicated. The upper concentration aptamers remain bound after the dissociation phase. The lower concentration aptamers dropped close to the base line. The resultant K_d was 16.9 nM ± 5.5.

After injection had stopped, the higher concentration aptamers (300 nM, 150 nM and 75 nM) remained stably bound to the protein after 100 seconds of dissociation while the lower concentration aptamers (5 nM to 37.5 nM) dropped almost to the base line (Figure 23). Although P2 did not bind HIV-1_{CAP45} gp120 with the highest RU, it had the strongest and most stable interaction.

Table 10: Calculated Constants and Associated Chi^2 Values for P2 Kinetics on HIV-1_{CAP45} gp120.

Flow Cell	k(off)	Chi^2	k(on)	Chi^2	K_d
1	6.47e-3	1.27	2.68e5	0	2.41e-8
2	5.68e-3	0.77	4.02e5	0	1.41e-8
3	4.61e-3	0.56	3.67e5	0	1.26e-8
AVERAGE	5.59e-3	0.86	3.46e5	0	1.69e-8

4. Discussion

As the aptamers were selected from such diverse libraries they were expected to form diverse structures. The predicted secondary structures differed in number predicted and conformation. Aptamer B84 had only one predicted structure which implied an increased level of certainty in the likelihood of that structure. The most structures were predicted for P2 (5 structures) which implied that the RNA may form arbitrary conformations other than that required for the aptamer. In turn, this may mean that the aptamer could be competed out by other, non binding structures. The difference between conformations was important for consideration as it indicated the diversity of the aptamer structures possible. P10 had the most overlapping bases (24 bases) between all four predicted conformations. P2 had the least overlaps (9 bases) which indicated diversity in possible conformations. The structure with the lowest ΔG was most likely of the predicted aptamer conformation. The lower the ΔG, the more inherently stable a conformation and the more likely it will form the basis of the tertiary structure required for aptamer binding. The most stable conformation as predicted by MFOLD was for B11 as it had the lowest ΔG value and three predicted conformations with significant overlaps. B65 was predicted with the least stable conformation with the largest ΔG of -11.30 and three predicted stable conformations that share no similarity.

As much as secondary structure provides an insight into the number of possible conformations and the predicted stabilities, it is the RNA in tertiary structure that interacts with the protein. To gain better insight into the RNA conformations an analysis of tertiary structure and the possible protein aptamer interaction could be addressed. This may have included, amongst others: RNAse digestion, circular dichroism, RNA footprinting and x-ray crystallography. RNAse digestion (Vary 1984) and circular dicroism (Hashizume 1967) can be used as methods to validate the predicted secondary structures. X-ray crystallography (Kim 1968) would provide tertiary structure information while RNA footprinting (Galas 1978) would provide information regarding the sequence motifs involved in protein binding.

Binding kinetic analysis reveals the relative strength of the aptamer-protein interaction. This has significant implications for the design of aptamer based therapeutics. A strong aptamer-protein interaction would have implications for both inhibitor and targeting aspects of aptamer based therapy. As an entry inhibitor, the stronger the aptamer binding is to gp120, the stronger the inhibition. This has been shown for antibody binding and neutralisation of SIV entry (Steckbeck 2005). Similarly, a strong aptamer-protein interaction

would increase contact time for the delivery of a therapeutic. The investigation of the binding kinetic properties of the aptamers identified them as highly diverse. A previous study by Dey et al (2005) reported a K_d of 31.3 ± 2 nM for B40t77 (truncated B40). This is similar to that of UCLA calculated between 33.9 nM and 35.2 nM. The similarity was expected as UCLA is a commercially available version of B40t77 modified for enhanced structural stability. The BIAcore user manual suggests using the lowest possible response units of immobilised protein. Previous studies (Khati 2003; Dey 2005) used 1000 RU, 5000 RU and 10 000 RU gp120 immobilised to the three experimental flow cells and none to a binding control flow cell. When these conditions were used, no aptamer binding was noted. This could be explained by the size of the gp120 protein. The bigger a binding molecule is, the higher the response units are with each individual molecule added. Thus the final response units have to be quite large for a larger molecule. By having a low response unit for gp120 binding there was not enough protein present on the chip for binding of the selected aptamers to occur.

When the UCLA optimised experimental conditions were repeated for (less characterised) aptamers B65, B19 and B84 the K_d could not be elucidated. The 1:1 Langmuir binding model showed an inverse in the graphs and no reading could be taken from them. This may indicate a saturation of the chip with the response units selected. At lower aptamer concentrations, the curves followed the expected gradient. When the concentration was increased, however, the graphs plummeted and ended below that of the lower concentration aptamers. This may indicate that the saturation point is reached early and the higher concentration was acting as to inhibit binding. When the concentration was increased the aptamers may have inhibited one another by competition and / or steric hindrance.

Using a further optimised protocol, the K_d of each aptamer was calculated. The K_d calculated for each aptamer can be seen in Table 11 below in order from smallest to largest with their associated ΔG as predicted by MFOLD. B40t77 was included as a standard for good gp120 binding kinetics. For the sake of comparison a standard deviation for UCLA was created from the results on 23 000 RU and 13 000 RU HIV-1_{DU151} gp120. Two aptamers (P2 and B84) showed a K_d smaller than that of B40t77 (Table 11). The majority of the aptamers were grouped within the same range of B40t77 with only P10 and B11 giving a much higher K_d (Table 11). B65 showed a K_d similar to that of B40t77 and although the statistical analysis provided Chi^2 values within the accepted range, the curve provided little confidence in the result. B65 was predicted with three completely different structures. This could indicate that the transcribed RNA did not fold into the aptamer conformation with great efficiency resulting in arbitrary conformations that confounded the result. Because of this B65 was not

considered a good candidate for further study. P2 and B84 were identified as the best candidates for further study as they have been shown to bind stably over time and have stable secondary structures when compared to the other aptamers.

Table 11: Comparison of Aptamer K_d and Most Probable Structure ΔG

Aptamer	K_d	ΔG
P2	16.9 nM ± 5.5	-19.72
B84	23 nM ± 8	-19.05
B40t77*	31.2 nM ± 2	-23.79
T58	33 nM ± 14	-18.4
UCLA#	34.5 nM ± 0.7	
B65	51 nM ± 8.5	-11.3
B11	179 nM ± 81	-26.8
P10	221 nM ± 81	-23.13

*B40t77 highlighted in red was included as a standard for aptamer dissociation, ΔG from MFOLD
#UCLA highlighted in orange has a standard deviation calculated from the 23 000 RU and 13 000 RU results, no ΔG was provided as MFOLD predictions do not account for additional modifications

The standard deviation for the calculated aptamers K_d is systematically higher than that for B40t77. This could be improved with more replicates as only three replicates were included in this study. Although the standard deviations are higher, they remain less than one third of the total indicating a tight grouping of results. The higher standard deviation can also be attributed to the use of only the BIAcore when calculating the K_d. The use of the BIAcore can induce variability in results if there are differences with the flow of the different flow cells on the chip. As the BIAcore is controlled by a nearby computer, there is little user interaction and thus one is reliant on its accuracy. By including more than one kinetic analysis method, the inherent variations could be reduced although experimental variation would persist. Numerous methods exist for the determination of binding kinetics, one of which is Quartz crystal microbalance with dissipation (QCM-D). QCM-D monitors a change in frequency as a result of added mass (Dixon 2008). This method can be used to detect a variety of interaction including: protein-protein, antibody-antigen and DNA-DNA (Dixon 2008). The drawback to this method is that it is only valid for rigid molecules as molecule movement could interrupt the detection of oscillations and that it requires molecules to be labelled for their immobilisation. This made the use of this technique for the purpose of this study

inappropriate. By labelling the molecules used, information can no longer be gained on native molecules and their interaction which could lead to misleading results and inaccurate conclusions. A great advantage to the use of SPR is the sensitivity to changes in mass and as such molecules do not need to be labelled for their interaction to be identified. Other advantages include that SPR can be used with relatively small amounts of materials and it provides a real time analysis of association and dissociation rates (Johnsson 1991; Crouch 1999). Initially there was intention of measuring the K_d using an Electro Mobility Shift Assay (EMSA) to corroborate the BIAcore results.

5. Further studies

With the time constraints on this project, all aspects of the aptamer protein interaction could not be explored. Outlined below are experiments that could be used to enhance the information gained from this project.

RNA footprinting and competition assays for the aptamers would be essential to elucidate the binding position on both the aptamer and the protein. RNA footprinting involves the degradation of the RNA while bound to the protein. The region bound to the protein is protected from degradation and can be detected by resolving on a non-denaturing gel (Galas 1978). By identifying the minimal sequence required for binding, aptamers can be truncated to include only the essential sequence. Smaller molecules are less affected by steric hindrance and can more easily navigate through the human body as a therapeutic. Aptamers of reduced size would be less expensive to produce which is an important consideration for large scale *in vitro* production. A competition assay would identify if the aptamer bound a known neutralising epitope or if it bind a novel site (Henry 1985). This would indicate its ability to be used in conjunction with other gp120 binding therapeutics.

Circular dichroism can be used to corroborate the secondary structures predicted by MFOLD. The signal detected differs if RNA molecules are folded in different orientations. This can be used to elucidate secondary structure information (Hashizume 1967).

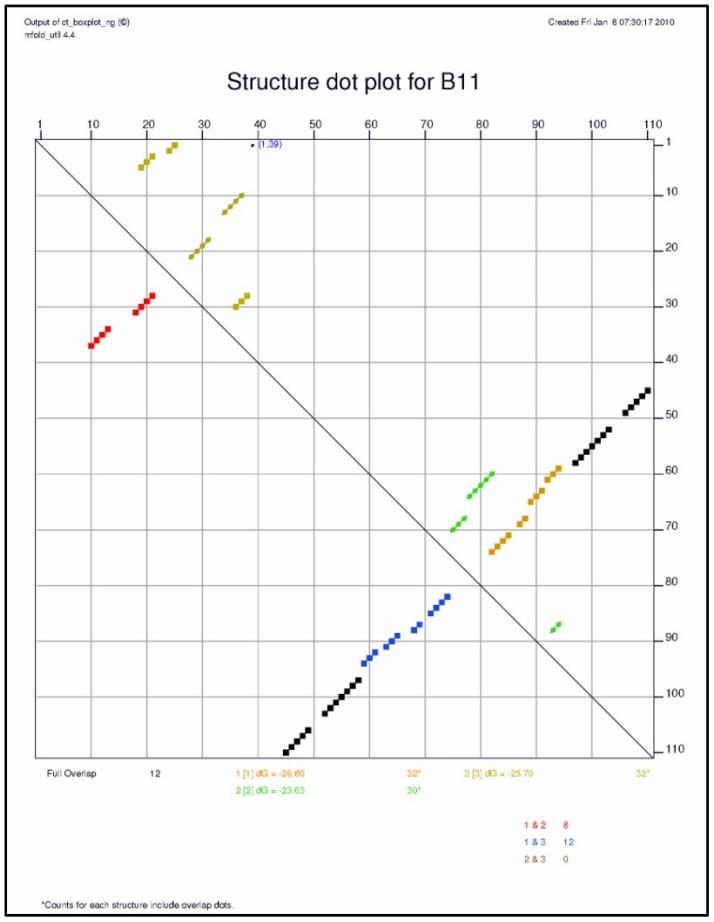
More than one kinetics analysis could be conducted to further strengthen the results obtained on the BIAcore. An EMSA could be conducted to provide this information. RNA-protein complexes are resolved on a polyacrylamide gel. A shift in band height between bound and non-bound RNA fractions corresponds to the concentration of the bound complex relative to the total RNA and protein concentration is solution. This shift can be quantified and used for the analysis of binding kinetics (Garner 1981).

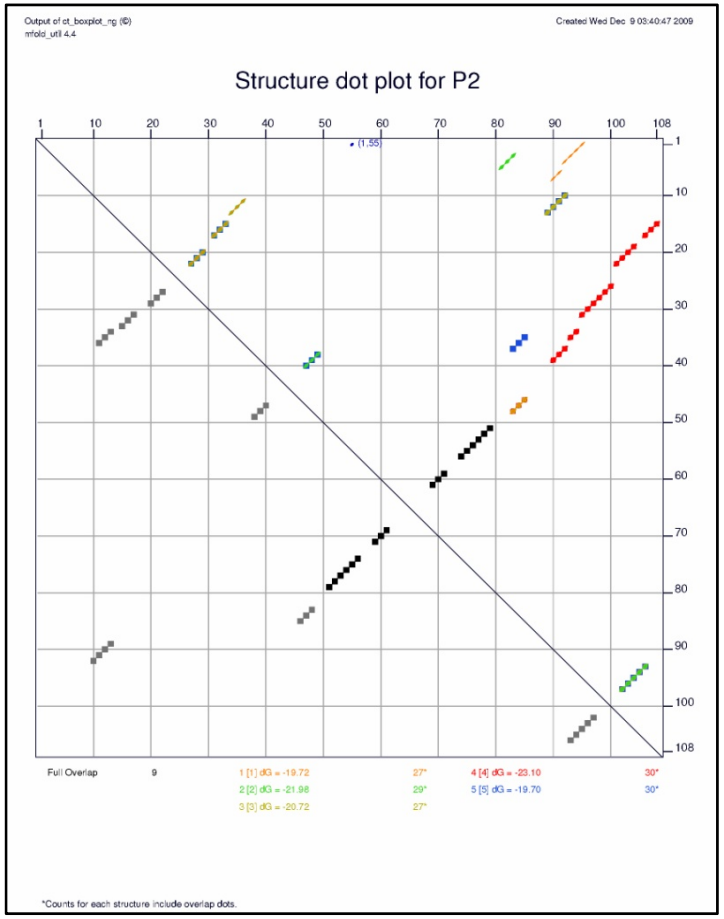
6. Conclusion

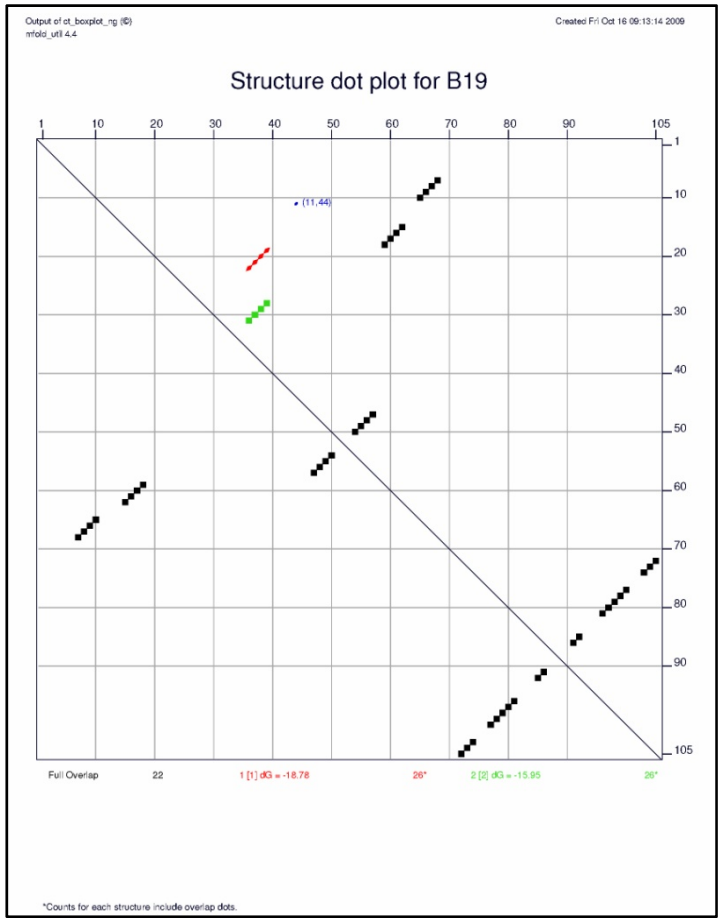
Structural stability and likelihood was based on the number of predicted structures, between structure similarity and associated structural ΔG values. B11 and B84 were identified as the most stable and B65 as the least stable aptamer. In the kinetic analysis, B11 and P10 were seen to have the highest dissociation constants of 179 nM ± 81 and 221 nM ±81 respectively. This indicates that they are possibly not good candidates for further analysis. The other aptamers had dissociation constants similar to or lower than B40t77 and so could be good candidates for further characterisation with exception of B65. Kinetic analysis of B65 indicated a similar dissociation constant to B40t77, a strong gp120 binding aptamer. Although the statistical analysis provided Chi^2 values within the accepted range, the curve provided little confidence in the result. The MFOLD predictions identified three possible structures with no structural similarity for B65. This may have resulted in the RNA in solution not forming the conformation required for binding. As such, B65 was identified as a poor candidate for further characterisation. The best binder with the lowest calculated dissociation constant was P2 with K_d = 16.9 nM ± 5.5. However, P2 was tested against monomeric gp120 from CAP45, the same viral strain to which it was raised. Further study of binding kinetics on proteins from other variants would provide further insight into its possible use. Five secondary structures were predicted for P2 with a portion of similarity between all of them. B84 was identified as the second best aptamer candidate with only one predicted structure and strong protein interaction (K_d =23 nM ± 8). The binding kinetics provides insight into the protein aptamer interaction strength. The lower the K_d of an aptamer, the stronger the interaction and more stable the binding. Aptamers with a low K_d could have improved bioavailability as they are able to bind their target for longer and avoid clearance from the body. This study has highlighted B84 and P2 as aptamers as possible therapeutic molecules for which further characterisation should follow.

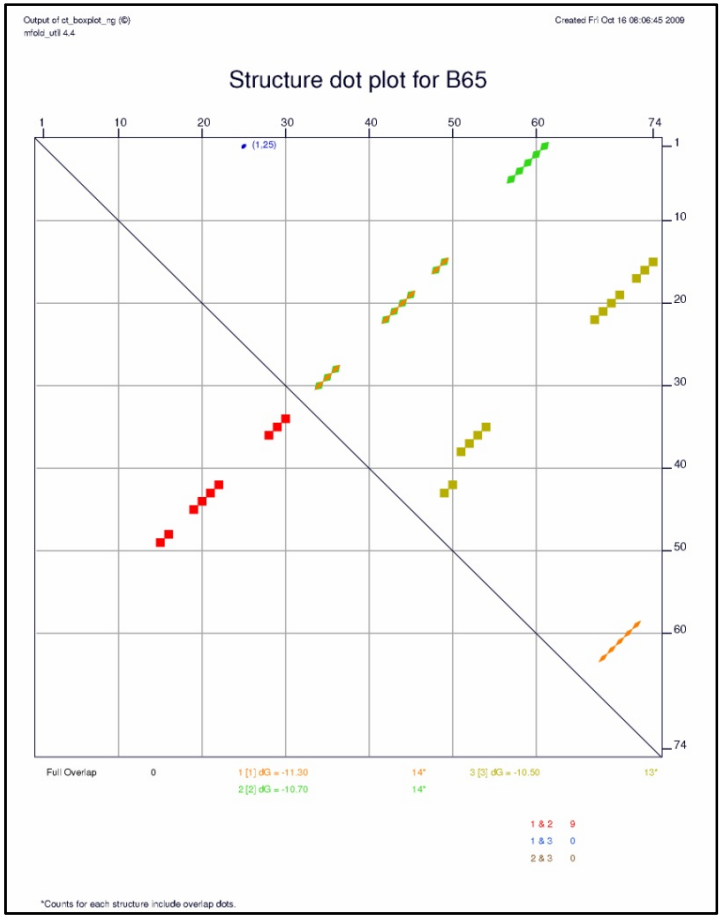
Appendix 1

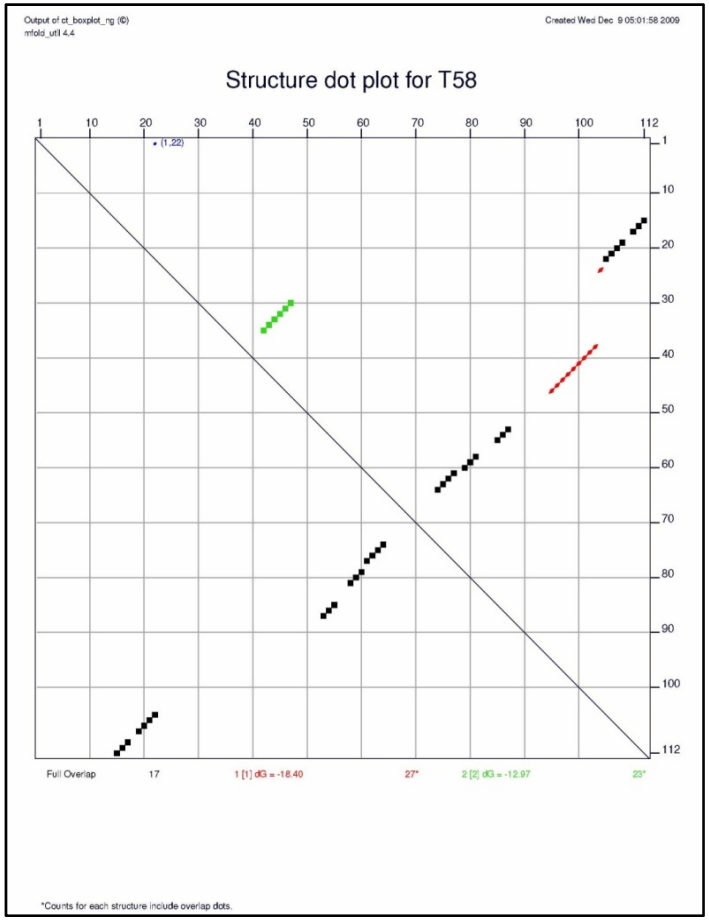
Structure Dot Plots for the aptamers with more than one predicted conformation. Structure dot plots indicate the aptamer name and the number of predicted structures. This in addition to the *pnum* and ΔG was used to determine the most stable and likely conformation.

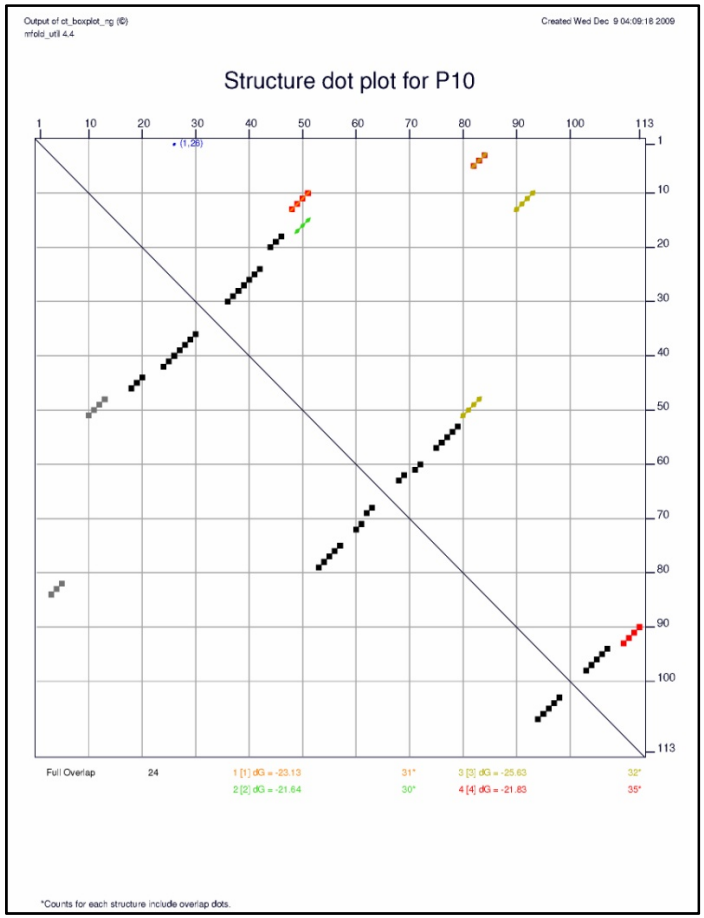





Output of ct_boxplot_ng (©)
rnfold_util 4.4
Created Fri Oct 16 09:13:14 2009
Structure dot plot for B19
(11,44)
Full Overlap 22
1 [1] dG = -18.78 26*
2 [2] dG = -15.95 26*
*Counts for each structure include overlap dots.


Output of ct_boxplot_ng (©)
rnfold_util 4.4
Created Fri Oct 16 08:06:45 2009
Structure dot plot for B65
(1,25)
Full Overlap 0
1 [1] dG = -11.30 14*
2 [2] dG = -10.70 14*
3 [3] dG = -10.50 13*
1 & 2 9
1 & 3 0
2 & 3 0
*Counts for each structure include overlap dots.


Output of ct_boxplot_ng (©)
mfold_util 4.4
Created Wed Dec 9 05:01:58 2009
Structure dot plot for T58
(1,22)
Full Overlap 17
1 [1] dG = -18.40 27*
2 [2] dG = -12.97 23*
*Counts for each structure include overlap dots.


Output of ct_boxplot_ng (©)
mfold_util 4.4
Created Wed Dec 9 04:09:18 2009
Structure dot plot for P10
(1,28)
Full Overlap 24
1 [1] dG = -23.13 31*
2 [2] dG = -21.64 30*
3 [3] dG = -25.63 32*
4 [4] dG = -21.83 35*
*Counts for each structure include overlap dots.

Appendix 2

Optimisation Experiments for Kinetics

B65 kinetic was determined on the UCLA optimised 13 000 RU HIV-1_{DU151} gp120. Three concurrent kinetics experiments were run on three flow cells loaded with 13 000 RU HIV-1_{DU151} gp120 with the fourth left empty as a no protein control. B65 binding appeared to fit the 1:1 Langmuir model however, on closer inspection it was noted that the graph had not followed the expected concentration gradient (Figure i). After injection the aptamer concentrations did not deviate in a concentration manner (Figure i). The second highest concentration (200 nM) resulted in maximum RU lower than the less concentrated aptamers (Figure i). At the start of dissociation there was a difference in aptamers of different concentrations. After 40 seconds the aptamer concentrations no longer deviated and 500 nM had the lowest RU (Figure i).

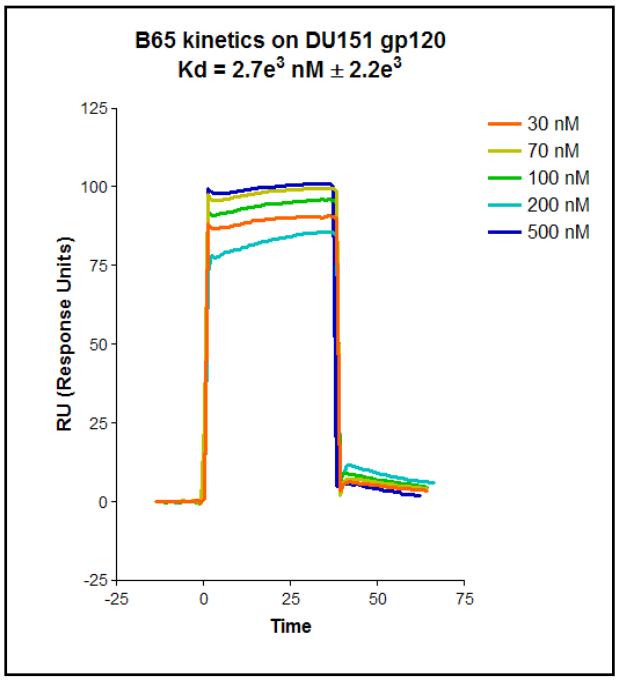


Figure i: B65 Binding Kinetics on 13 000 RU HIV-1_{DU151} gp120.
The aptamer concentrations did not diverge from one another in the expected pattern. The concentrations were too close for adequate analysis. As such, the calculated K_d of $2.7e^3$ cannot be taken as an accurate result even though the Chi^2 analysis showed the results to be significant.

The average dissociation constant was calculated and the standard deviation was determined (Table i). There was a large variation in calculated K_d for each flow cell. Using the separate ka / kd calculation, B65 was shown to have a $K_d = 2.7e^3$ nM ± $2.2e^3$. The Chi^2 calculated for the experiment fit within a reasonable range which indicated statistical significance. The

values were similar between two flow cells with one as an outlier for all three calculations. The large standard deviation was testament to the high variability between flow cells. When analysed with the simultaneous ka / kd, the Chi^2 value was more than two orders of magnitude higher and the K_d more than two orders of magnitude lower. Due to the lack of deviation between concentrations it was concluded that the concentrations were too similar for a reliable calculation to be generated. As 500 nM proved to be too concentrated for aptamer binding, the upper limit concentration would start at 200 nM and reduce in half log dilutions.

Table i: Calculated Constants and Associated Chi^2 values for B65 Kinetics on HIV-1_{DU151} gp120

Flow Cell	k(off)	Chi^2	k(on)	Chi^2	K_d
1	0.0226	0.0167	2.4e4	0.01	9.4e-7
2	0.0309	0.0197	1.72e4	0.01	1.79e-6
3	0.0329	0.006	5.82e-3	0.007	5.66e-6
Average					2.7e-6

The experiment was repeated for B19 (excluding 500 nM) to test if another aptamer would follow the same trend. B19 fit the 1:1 Langmuir Binding model to the same extent as B65. The kinetics graph followed the same general trend with the different concentrations clumping together (Figure ii). The more concentrated aptamer samples grouped at almost the same response unit level while 30 nM ended much lower down (Figure ii).

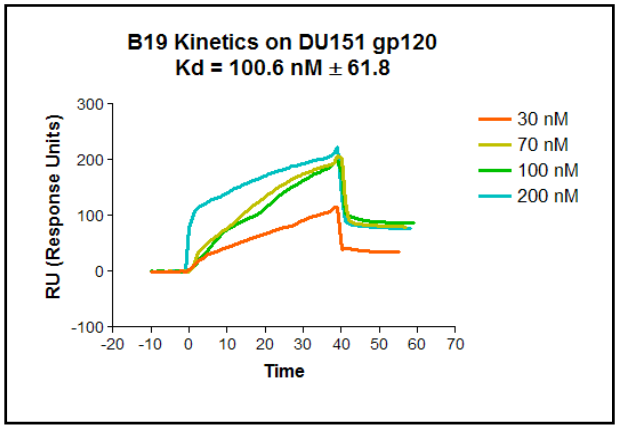


Figure ii: B19 Binding Kinetics on HIV-1_{DU151} gp120.
The coloured lines indicate the aptamer concentrations injected. The upper concentrations for B19 clumped together while 30 nM was very distinct. The calculated K_d = 100 nM ± 61.8.

The K_d was calculated and the standard deviation determined with the associated Chi^2 values (Table ii). The K_d was calculated as 100.6 nM ± 61.8. Again a very high standard deviation was seen, this was attributed to injected aptamer concentrations being indistinguishable which lead to an inaccuracy in the calculations. When calculating the k(on), the concentration is an important factor and since there was no concentration variation, this may have introduced an error into the calculation.

Table ii: Calculated Constants and Associated Chi^2 values for B19 Kinetics on HIV-1_{DU151} gp120

Flow Cell	k(off)	Chi^2	k(on)	Chi^2	K_d
1	2.9e-3	0.070	1.40e5	0	2.08e-8
2	6.35e-3	0.101	4.54e4	0	1.4e-7
3	0.0128	0.995	9.08e4	0	1.41e-7
Average	7.35e3	0.398	9.21e4	0	1.0e-7

Associated Graphs for B84 Optimisation on DU151

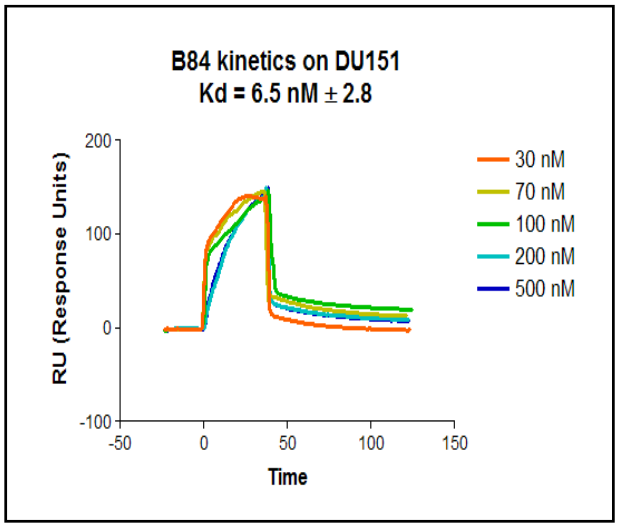


Figure iii: B84 Binding Kinetics on HIV-1_{DU151} gp120.
B84 fits 1:1 Langmuir binding model and the binding curve does not the expected line. Higher concentrations group together with 200 nM and 500 nM below 70 nM and 100 nM. 30 nM ends with the lowest response units as expected. The dissociation constant was calculated by taking the average of three concurrent experiments and the standard deviation was determined. B84 is shown to be a tight binder with Kd = 6.5 nM ± 2.8.

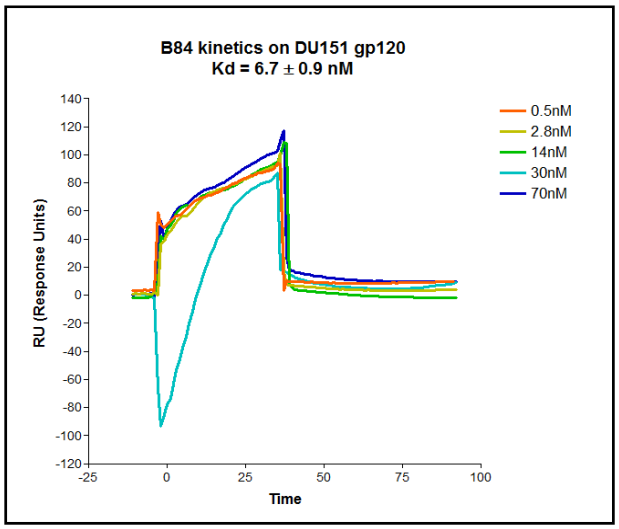


Figure iv: B84 Kinetics on HIV-1_{DU151} gp120 with reduced aptamer concentration.
To overcome the problems with saturation found with previous experiments, a reduced aptamer concentration was used. Half log dilutions from 70 nM to 0.5 nM were prepared and run on a chip loaded with 10 000 RU. Aptamer concentrations below 14 nM appeared to be below the limit of detection and thus the curve did not follow the expected gradient for all concentrations.

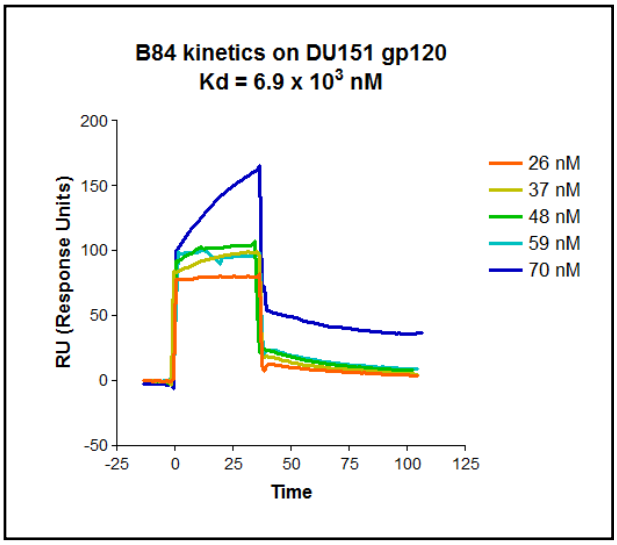


Figure v: B84 kinetics on HIV-1_{DU151} gp120 with reduced concentration limits.
The previously determined concentration limits were established and concentrations between were chosen. Six data points were used in the determination of the dissociation constant. These points appear to be too similar to provide meaningful results. The upper limit for kinetics must be raised to allow for a larger difference between sample concentrations.

Reference List

Andreola, M., Pileur, F., Calmels, C., Ventura, M., Tarrago-Litvak, L., Toulme, J., and Litvak, S. (2001). "DNA Aptamers Selected Against the HIV-1 RNAse H Display *in vitro* Antiviral Activity." Biochemistry **40**: 10087-10094.

Arbuthnot, P., Longshaw, V., Naidoo, T., and Weinberg, M.S. (2007). "Opportunities for Treating Chronic Hepatitis B and C Virus Infection Using RNA Interference." Journal of Viral Hepatitis **14**: 447-459.

Barichievy, S., Saayman, S., Von Eije, K.J., Morris, K.V., Arbuthnot, P., and Weinberg, M.S. (2007). "The Inhibitory Efficacy of RNA POL III-Expressed Long Hairpin RNAs Targeted to Untranslated Regions of the HIV-1 5' Long Terminal Repeat." Oligonucleotides **17**: 419-431.

Baxter, J. D., Schapiro, J.M., Boucher, C.A.B., Kohlbrenner, V.M., Hall, D.B., Scherer, J.R., and Mayers D.L. (2006). "Genotypic Changes in Human Immunodeficiency Virus Type 1 Protease Associated with Reduced Susceptibility and Virologic Response to the Protease Inhibitor Tipranavir." Journal of Virology **80**(21): 10794-10801.

Berezovski, M. V., Lechmann, M., Musheev, M.U., Mak, T.W., and Krylov, S.N. (2008). "Aptamer-Facilitated Biomarker Discovery (AptaBiD)." American Chemical Society **130**(9137-9143).

Biscone, M. J., Pierson, T.C., and Doms, R.W. (2002). "Opportunities and Challenges in Targeting HIV Entry." Current Opinion in Pharmacology **2**(5): 529-533.

Boutros, M., and Ahringer, J. (2008). "The Art and Design of Genetic Screens: RNA Interference." Nature **9**: 554-566.

Briz, V., Poveda, E., and Soriano, V. (2006). "HIV Entry Inhibitors: Mechanisms of Action and Resistance Pathways." Journal of Antimicrobial Chemotherapy **57**: 619-627.

Burton, D. R., Pyati, J., Koduri, R., Sharp, S.J., Thornton, G.B., Parren, P.W., Sawyer, L.S., Hendry, R.M., Dunlop, N., and Nara, P.L. (1994). "Efficient neutralization of primary isolates of HIV-1 by a recombinant human monoclonal antibody." Science **266**: 1024-1027.

Castanotto, D., and Rossi, J.J. (2009). "The Promises and Pitfalls of RNA-Interference-Based Therapeutics." Nature **457**: 426-433.

Cave, E., Weinberg, M.S., Cilliers, T., Morris, L., and Arbuthnot, P. (2006). "Silencing of HIV-1 Subtype C Primary Isolates by Expressed Small Hairpin RNAs Targeted to gag." AIDS Research and Human Retroviruses. **22**(5): 401-410.

Chan, D. C., Fass, D., Berger, J.M., and Kim, P.S (1997). "Core Structure of gp41 from the HIV Envelope Glycoprotein." Cell Press **89**: 263-273.

Chan, S. Y., Speck, R.F., Power, C., Gaffen, S.L., Chesebro, B., and Goldsmith, M.A. (1999). "V3 Recombinants Indicate a Central Role for CCR5 as a Coreceptor in Tissue

Infection by Human Immunodeficiency Virus Type 1." Journal of Virology **73**(3): 2350-2358.

Chen, Y., Cheng, G., and Mahato, R.I. (2008). "RNAi for Treating Hepatitis B Viral Infection." Pharmaceutical Research **25**(1): 72-86.

Cohen, C., Forzan, M., Sproat, B., Pantophlet, R., McGowan, I., Burton, D., and James, W. (2008). "An aptamer that neutralises R5 strains of HIV-1 binds to core residues of gp120 in the CCR5 binding site " Virology **381**(1): 46-54.

Crouch, R. J., Wakasa, M., and Haruki, M. (1999). Detection of Nucleic Acid Interactions Using Surface Plasmon Resonance. RNA-Protein Interaction Protocols. S. R. Haynes. New York, Humana Press. **118**.

Darfeuille, F., Hansen, J.B., Orum, H., Di Primo, C., and Toulme, J. (2004). "LNA/DNA Chimeric Oligomers Mimic RNA Aptamers Targeted to the TAR RNA Element of HIV-1." Nucleic Acids Research **32**(10): 3101-3107.

de Soultrait, V. R., Lozach, P., Altmeyer, R., Tarrago-Litvak, L., Litvak, S., and Andreola, M.L. (2002). "DNA Aptamers Derived from HIV-1 RNase H Inhibitors are Strong Integrase Agents." Journal of Molecular Biology **324**: 195-203.

Dey, A. K., Griffiths, C., Lea, S.M., and James, W. (2005). "Structural Characterisation of an Anti-gp120 RNA Aptamer that Neutralises R5 Strains of HIV-1." RNA **11**: 873-884.

Dhar, S., Gu, F.X., Langer, R., Farkhozad, O.C., and Lippard, S.J. (2008). "Targeted Delivery of Cisplatin to Prostate Cancer Cells by Aptamer Functionalised Pt(IV) Prodrug-PLGA_PEG Nanoparticles." PNAS **105**(45): 17356-17361.

Dixon, M. C. (2008). "Quartz Crystal Microbalance with Dissipation Monitoring: Enabling Real-Time Characterisation of Biological Materials and their Interactions." Journal of Biomolecular Technology **19**(3): 151-158.

Djordjevic, M. (2007). "SELEX Experiments: New Prospects, Applications and Data Analysis in Inferring Regulatory Pathways." Biomolecular Engineering **24**: 179-189.

Dorr, P., Westbly, M., Dobbs, S., Griffin, P., Irvine, B., Macartney, M., Mori, J., Rickett, G., Smith-Burchnell, C., Napier, C., Webster, R., Armour, D., Price, D., Stammen, B., Wood, A., and Perros, M. (2005). "Maraviroc (UK-427,857), a Potent, Orally Bioavailable, and Selective Small-Molecule Inhibitor of Chemokine Receptor CCR5 with Broad-Spectrum Anti-Human Immunodeficiency Virus Type 1 Activity." Antimicrobial Agents and Chemotherapy **49**(11): 4721-4732.

Duconge, F., and Toulme, J.J. (1999). "*In vitro* Selection Identifies Key Determinants for Loop-Loop Interactions: RNA Aptamers Selective for the TAR RNA Element of HIV-1." RNA **5**: 1605-1614.

Eaton, B. E., Gold, L., Zichi, D.A. (1995). "Let's Be Specific: The Relationship Between Specificity and Affinity." Chemical Biology **2**: 633-638.

Ellington, A. D., and Szostak, J.W. (1990). "*In vitro* Selection of RNA Molecules that Bind Specific Ligands." Nature **346**: 818-822.

Este, J. A., and Telenti, A. (2007). "HIV Entry Inhibitors." The Lancet **370**(9581): 81-88.

Este, J. A., Cabrera, C., Blanco, J., Gutierrez, A., Bridger, G., Henson, G., Clotet, B., Schols, D., and De Clercq, E. (1999). "Shift of Clinical Human Immunodeficiency Virus Type 1 Isolates from X4 to R5 and Prevention of Emergence of the Syncytium-Inducing Phenotype by Blockade of CXCR4 " Journal of Virology **73**(7): 5577-5585.

Eugene, W. M., and Adamis, A.P. (2005). "Targeting angiogenesis, the underlying disorder in neovascular age-related macular degeneration." Canadian Journal of Ophthalmology **40**: 352-368.

Felgner, P. L., Gadek, T.R., Holm, M., Roman, R., Chan, H.W., Wenz, M., Northrop, J.P., Ringold, G.M., and Danielsen, M. (1987). "Lipofection: A Highly Efficient, Lipid-Mediated DNA-Transfection Procedure." Proceedings of the National Academy of Sciences of the United States of America **84**(21): 7413-7417.

Flexner, C. (2007). "HIV Drug Development: The Next 25 Years." Nature **6**: 959-966.

Frey, G., Peng, H., Rits-Volloch, S., Morelli, M., Cheng, Y., and Chen, B. (2008). "A Fusion-Intermediate State of HIV-1 gp41 Targeted by Broadly Neutralizing Antibodies." PNAS **105**(10): 3739-3744.

Galas, D. J., and Schmitz, A. (1978). "DNAase Footprinting: A Simple Method for Detection of Protein-DNA Binding Specificity." Nucleic Acid research **5**(9): 3157-3170.

Gallo, S. A., Finnegan, C.M., Viard, M., Raviv, Y., Dimitrov, A., Rawat, S.S., Puri, A., Durell, S., and Blumenthal, R. (2003). "The HIV Env-Mediated Fusion Reaction." Biochimica et Biophysica Acta **1614**: 36-50.

Garner, M. M., and Revzin, A. (1981). "A Gel Electrophoresis Method for Quantifying the Binding of Proteins to Specific DNA Regions: Application to Components of the Escherichia coli Lactose Operon Regulatory System." Nucleic Acids Research **9**(13): 3047-3060.

Gopinath, S. C. B., Balasundaresan, D., Akitomi, J., and Mizuno, H. (2006). "An RNA Aptamer That Discriminates Bovine Factor IX from Human Factor IX." Journal of Biochemistry **140**(5): 667-676.

Gorny, M. K., Williams, C., Volsky, B., Revesz, K., Cohen, S., Polonis, V.R., Honnen, W.J., Kayman, S.K., Krachmarov, C., Pinter, A., and Zolla-Pazner, S. (2002). "Human Monoclonal Antibodies Specific for Conformation-Sensitive Epitopes of V3 Neutralize Human Immunodeficiency Virus Type 1 Primary Isolates from Various Clades." Journal of Virology **76**(18): 9035-9045.

Gragoudas, E. S., Adamis, A.P., Cunningham, E.T., Feinsod, M., and Guyer, D.R. (2004). "Pegaptanib for Neovascular Age-Related Macular Degeneration." The New England Journal of Medicine **351**(27): 2805-2816.

Hage, D. S. (1999). "Affinity Chromatography: A Review of Clinical Applications." Clinical Chemistry **45**(5): 593-615.

Hammer, S. M., Eron, J.J., Reiss, P., Schooley, R.T., Thompson, M.A., Walmsley, S., Cahn, P., Fischl, M.A., Gatell, J.M., Hirsch, M.S., Jacobsen, D.M., Montaner, J.S.G., Richman, D.D., Yeni, P.G., and Volberding, P.A. (2008). "Antiretroviral Treatment of Adult HIV Infection." The Journal of the American Medical Association **300**(5): 555-570.

Hashizume, H., and Imahori, K. (1967). "Circular Dichroism and Conformation of Natural and Synthetic Polynucleotides." Japanese Biochemical Society **61**(6): 738-749.

Hemelaar J., G. E., Ghys P.D., and Osmanov S. (2006). "Global and regional distribution of HIV-1 genetic subtypes and recombinants in 2004." AIDS **20**: W13-W23.

Henry, R. M., Fernie, B.F., Anderson, L.J., Godfrey, E., and McIntosh, K. (1985). "Monoclonal Capture Antibody ELISA for Respiratory Syncytial Virus: Detection of Individual Antigens and Determination of Monoclonal Antipody Specificities." Journal of Immunological Methods **77**(2): 247-258.

Jacobs, A., Garg, H., Viard, M., Raviv, Y., Puri, A., and Blumenthal, R. (2008). "HIV-1 Envelope Glycoprotein-Mediated Fusion and Pathogenesis: Implications for Therapy and Vaccine Development." Vaccine **26**(24): 3026-3035.

James, W. (2001). "Nucleic Acid and Peptide Aptamers: A Powerful Approach to Ligand Discovery." Current Opinion in Pharmacology **1**: 540-546.

Jenison, R. D., Gill, S.C., Pardi, A., and Polisky, B. (1994). "High-resolution Molecular Discrimination by RNA." Science **263**(5152): 1425-1429.

Johnsson, B., Löfås, S., and Lindquist, G. (1991). "Immobilization of Proteins to a Carboxymethyldextran-Modified Gold Surface for Biospecific Interaction in Surface Plasmon Resonance Sensors." Analytical Biochemistry **198**: 268-277.

Kelker, H. C., Itri, V.R., and Valentine, F.T. (2010). "A Strategy for Eliciting Antibodies against Cryptic, Conserved, Conformationally Dependent Epitopes of HIV Envelope Glycoprotein." PLOS one **5**(1): e8555.

Khati, M., Schuman, M., Ibrahim, J., Sattentau, Q., Gordon, S., and James, W. (2003). "Neutralisation of Infectivity of Diverse R5 Clinical Isolates of Human Immunodeficiency Virus Type 1 by gp120-Binding 2'F-RNA Aptamers." Journal of Virology **77**(23): 12692-12698.

Kim, S., and Rich, A. (1968). "Single Crystals of Transfer RNA: An X-Ray Diffraction Study." Science **162**(3860): 1381-1384.

Li, N., Wang, Y., Pothukuchy, A., Syrett, A., Husain, N., Gopalakrisha, S., Kosaraju, P., and Ellington, A.D. (2008). "Aptamers that Recognize Drug-Resistant HIV-1 Reverse Transcriptase." Nucleic Acids Research **36**(21): 6739-6751.

Liu, J., Bartesaghi, A., Borgnia, M.J., Sapiro, G., and Subramaniam, S. (2008). "Molecular Architecture of Naitive HIV-1 gp120 Trimers." Nature **455**(7209): 109-113.

Meissner, E. G., Zhang, L., Jiang, S., and Su, L. (2006). "Fusion-Induced Apoptosis Contributes to Thymocyte Depletion by a Pathogenic Human Immunodeficiency Virus Type 1 Envelope in the Human Thymus." Journal of Virology **80**(22): 11019-11030.

Mello, M. A. G., Mascarenhas, R.E., Ferraro, G.A., Harn, D., Galvao-Castro, B., and Bou-Habib, D.C. (2005). "Inhibition of HIV-1 Infection by Monoclonal Antibodies to Carbohydrates of *Schistosoma mansoni*." Medical Microbiology and Immunology **194**: 61-65.

Miller, M. D., Geleziunas, R., Bianchi, E., Lennard, S., Hrin, R., Zhang, H., Lu, M., An, Z., Ingallinella, P., Finotto, M., Mattu, M., Finnefrock, A.C., Bramhill, D., Cook, J., Eckert, D.M., Hampton, R., Patel, M., Jarantow, S., Joyce, J., Ciliberto, G., Cortese, R., Lu, P., Strohl, W., Schleif, W., McElhaugh, M., Lane, S., Lloyd, C., Lowe, D., Osbourn, J., Vaughan, T., Emini, E., Barbato, G., Kim, P.S., Hazuda, D.J., Shiver, J.W., and Pessi, A. (2005). "A Human Monoclonal Antibody Neutralizes Diverse HIV-1 Isolates by Binding a Critical gp41 Epitope." PNAS **102**(41): 14759-14764.

Montagnier, L., Clavel, F., Krust, B., Chamaret, S., Rey, F., Barre-Sinoussi, F., and Chermann, J.C. (1985). "Identification and Antigenicity of the Major Envelope Glycoprotein of Lymphadenopathy-Associated Virus." Virology **144**(1): 283-289.

Morris, L., and Cilliers, T. (2005). Viral Structure, Replication, Tropism, Pathogenesis and Natural History. HIV/AIDS in South Africa, Cambridge University Press.

Moyle, G., DeJesus, E., Boffito, M., Wong, R.S., Gibney, C., Badel, K., MacFarland, R., Calandra, G., Bridger, G., and Becker, S. (2009). "Proof of Activity with AMD11070, an Orally Bioavailable Inhibitor of CXCR4-Tropic HIV Type 1." Clinical Infectious Diseases **48**: 798-805.

Nowak, J. Z. (2006). "Age-related macular degenreation (AMD) pathogenesis and therapy." Pharmacological Reports **58**: 353-363.

O'Sullivan, C. K. (2002). "Aptasensors - The Future of Biosensing?" Analytical and Bioanalytical Chemistry **372**: 44-48.

Osborne, S. E., Matsumura, I., and Ellington, A.D. (1997). "Aptamers as Therapeutic and Diagnostic Reagents: Problems and Prospects." Current Opinion in Chemical Biology **1**: 5-9.

Pastore, C., Nedellec, R., Ramos, A., Pontow, S., Ratner, L., and Mosier, D.E. (2006). "Human Immunodeficiency Virus Type 1 Coreceptor Switching: V1/V2 Gain-of-Fitness Mutations Compensate for V3 Loss-of-Fitness Mutations." Journal of Virology **80**(2): 750-758.

Penedoa, F. J., Gonzaleza, J.S., Dahna, J.R., Antonia, M., Malowb, R., Costac, P., and Schneidermana, N. (2003). "Personality, quality of life and HAART adherence among men and women living with HIV/AIDS." Journal of Psychosomatic Research **54**: 271-278.

Phogat, S., Wyatt, R.T., and Karlsson Hedestam, G.B. (2007). "Inhibition of HIV-1 Entry by Antibodies: Potential Viral and Cellular Targets." Journal of Internal Medicine **262**(1): 26-43.

Raja, A., Venturi, M., Kwong, P., and Sodroski, J. (2003). "CD4 Binding Site Antibodies Inhibit Human Immunodeficiency Virus gp120 Envelope Glycoprotein Interaction with CCR5." Journal of Virology **77**: 713-718.

Robertson, D. (2003). "US FDA Approves New Class of HIV Therapeutics." Nature Biotechnology **21**: 470-471.

Saayman, S., Barichievy, S., Capovilla, A., Morris, K.V., Arbunthnot, P., and Weinberg, M.S. (2008). "The Efficacy of Generating Three Independent Anit-HIV-1 siRNAs from a Single U6 RNA Pol III-Expressed Long Hairpin RNA." PLOS Online **3**(7): 1-10.

Sampson, T. (2003). "Aptamers and SELEX: The Technology." World Patent Information **25**: 123-129.

Sayer, N., Ibrahim, J., Turner, K., Tahiri-Alaoui, A., and James, W. (2002). "Structural Characterization of a 2'F-RNA Aptamer that Binds a HIV-1 SU Glycoprotein, gp120." Biochemical and Biophysical Research Communications **293**: 924-931.

Siomi, H., and Siomi, M.C. (2009). "On the Road to Reading the RNA-Interference Code." Nature **475**: 396-404.

Stamatatos, L., Morris, L., Burton, D.R., and Mascola, J.R. (2009). "Neutralising Antibodies Generated During HIV-1 Infection: Good News for HIV-1 Vaccine?" Nature Medicine **15**: 866-870.

Starcich, B. R., Hahn, B.H., Shaw, G.M, McNeely, P.D., Modrow, S., Wolf, H., Parks, W.P., Josephs, S.F and Gallo, R.C. (1986). "Identification and Characterisation of Conserved and Variable regions in the envelope gene of HTLV-III/LAV, the retrovirus of AIDS." Cell **45**(5): 637-648.

Steckbeck, J. D., Orlov, I., Chow, A., Grieser, H., Miller, K.,Bruno, J., Robinson, J.E., Montelaro, R.C., and Cole, K.S. (2005). "Kinetic Rates of Antibody Binding Correlate with Neutralization Sensitivity of Variant Simian Immunodeficiency Virus Strains." Journal of Virology **79**(19): 12311-12320.

Stenger, M. (2009). Antiretroviral Therapy: New Drugs, Formulations, Ideas, and Strategies. Top HIV Medicine. D. Eron. Chicago, International AIDS Society. **17:** 146-150.

Stoltenburg, R., Reinemann, C., and Strehlitz, B. (2007). "SELEX- A (R)evolutionary Method to Generate High-Affinity Nucleic Acid Ligands." Biomolecular Engineering **24**: 381-403.

Teurk, C., and Gold, L. (1990). "Systematic Evolution of Ligands by Exponential Enrichment: RNA Ligands to Bacteriophage T4 DNA Polymerase." Science **249**: 505-510.

Trkola, A., Pomales, A.B., Yuan, H., Krober, B., Maddon, P.J., Allaway, G.P., Katinger, H., Barbas, C.F., Burton, D.R., Ho, D.D. et al. (1995). "Cross-clade neutralization of primary

isolates of human immunodeficiency virus type 1 by human monoclonal antibodies and tetrameric CD4-IgG." Journal of Virology **69**: 6609-6617.

Ulrich, H., Trujillo, C.A., Nery, A.A., Alves, J.M., Majumder, P., Resende, R.R., and Martins, A.H. (2006). "DNA and RNA Aptamers: From Tools for Basic Research Towards Theraputic Applications." Combinatorial Chemistry and High Throughput Screening **9**: 619-632.

Umekage, S., and Kikuchi, Y. (2009). "*In vitro* and *in vivo* Production and Purification of Circular RNA Aptamer." Journal of Biotechology **139**: 265-272.

UNAIDS (2009). "AIDS Epidemic Update."

Urchil, P., and Mothes, W. (2009). "HIV Entry Revisited." Cell **137**(3): 402-404.

Vary, C. P. H., and Vournakis, J.N. (1984). "RNA Structure Analysis Using Methidiumpropyl-EDTA.Fe(II): A Base-Pair-Specific RNA Structure Probe." Proceedings of the National Academy of Sciences **81**: 6978-6982.

Vergne, L., Peeters, M., Mpoudi-Ngole, E., Bourgeois, A., Liegeois, F., Toure-Kane, C., Mboup, S., Mulanga-Kabeya, C., Saman, E., Jourdan, J., Reyens, J., and Delaporte, E. (2000). "Genetic Diversity of Protease and Reverse Transcriptase Sequences in Non-Subtype-B Human Immunodeficiency Virus Type 1 Strains: Evidence of Many Minor Drug Resistance Mutations in Treatment-Naive Patients." Journal of Clinical Microbiology **38**(11): 3919-3925.

Wei, W., and Ling-Yun, J. (2009). "Progress in Aptamer Screening Methods." Chinese Journal of Analytical Chemistry **37**(3): 454-460.

Weinberg, M. S., and Wood, M.J.A. (2009). "Short Non-Coding RNA Biology and Neurodegenerative Disorders: Novel Disease Targets and Therapeutics." Human Molecular Genetics **18**(R1): R27-R39.

Weissenhorn, W., Dessen, A., Harrisson, S.C., Skehel, J.J., and Wiley, D.C. (1997). "Atomic structure of the Ecotodomain from HIV-1 gp41 " Nature **387**: 426-430.

Wild, C. T., McDanal, C.B., Bolognesi, D., and Matthews, T.J. (1992). "A Synthetic Peptide Inhibitor of Human Immunodeficiency Virus Replication: Correlation Between Solution Structure and Viral Inhibition." Proceedings of the National Academy of Sciences **89**(21): 10537-10541.

Wild, C. T., Shugars, D.C., Greenwell, T.K., McDanal, C.B., and Matthews, T.J. (1994). "Peptides Corresponding to a Predictive Alpha-Helical Domain of Human Immunodeficiency Virus Type 1 gp41 are Potent Inhibitors of Virus Infection." Proceedings of the National Academy of Sciences **91**(21): 9770-9774.

Xiao, Z., Shangguan, D., Cao, Z., Fang, X., and Tan, W. (2008). "Cell-Specific Internalization Study of an Aptamer from Whole Cell Selection." Chemistry a European Journal **14**: 1769-1775.

Yan, A. C., and Levy, M. (2009). "Aptamers and Aptamer Targeted Delivery." RNA Biology **6**(3): 316-320.

Yang, Y., Yang, D., Schluesener, H.J., and Zhang, Z. (2007). "Advances in SELEX and Application of Aptamers in the Central Nervous System." Biomolecular Engineering **24**: 583-592.

Zhang, Z., Blank, M., and Schluesener, H.J. (2004). "Nucleic Acid Aptamers in Human Viral Disease." Archivum Immunologiae et Therapiae Experimentalis **52**: 307-315.

Zhou, J., Swiderski, P., Li, H., Zhang, J., Neff, C.P., Akkina, R., and Rossi, J.J. (2009). "Selection, Characterisation and Application of New RNA HIV gp120 Aptamers for Facile Delivery of Dicer Substrate siRNAs into HIV Infected Cells." Nucleic Acid research **37**(9): 3094-3109.

Zuker, M. (2003). "Mfold Web Server for Nucleic Acid Folding and Hybridization Prediction." Nucleic Acids Research **31**(13): 3406-3415.

Zwick, M. B., Labrijn, A.F., Wang, M., Spenlehauer, C., Saphire, E.O., Binley, J.M., Moore, J.P., Stiegler, G., Katinger, H., Burton, D.R., and Parren, P.W.H.I. (2001). "Broadly Neutralizing Antibodies Targeted to the Membrane-Proximal External Region of Human Immunodeficiency Virus Type 1 Glycoprotein gp41." Journal of Virology **75**(22): 10892-10905.

Zwick, M. B., Saphir, E.O., and Burton, D.R. (2004). "gp41: HIV's Shy Protein." Nature Medicine **10**(2): 133-134.